# **CAAP Annual Report**

**Date of Report**: 09/30/2025

**Prepared for**: U.S. DOT Pipeline and Hazardous Materials Safety Administration

**Annual Period:** From (September 30, 2024) to (September 29, 2025)

Contract Number: 693JK32250008CAAP

Project Title: Performance Evaluation and Risk Assessment of Excessive Cathodic

Protection on Vintage Pipeline Coatings

**Prepared by**: *Qixin Zhou, Qindan Huang, and Hao Wang* 

Contact Info.: *Qixin Zhou* @uakron.edu, 330-972-7159

Qindan Huang, qindan.huang@marquette.edu, 414-288-6670

Hao Wang, hw261@soe.rutgers.edu, 848-445-2874

# **Table of Contents**

Tab	ole of Con	tents	2
Sec	tion A: B	usiness and Activities	3
Sec	tion B: De	etailed Technical Results in the Report Period	7
		sk 1. Identification of Vintage Pipeline Coatings and Influencing Factors in C c Disbondment	_
		sk 2. Evaluation of Coating Cathodic Disbondment Considering Key Influenthrough Laboratory Testing	_
	2.1.	Background and Objectives in the 3 <sup>rd</sup> Annual Report Period	7
	2.2.	Research Progress in the 3 <sup>rd</sup> Annual Report Period	7
	2.3.	Conclusions	16
	2.4.	Future Work	17
		sk 3. Numerical Simulation of Pipeline Coating Disbondment Behavior as	
	3.1.	Background and Objectives in the 3 <sup>rd</sup> Annual Report Period	18
	3.2.	Research Progress in the 3 <sup>rd</sup> Annual Report Period	18
	3.3.	Conclusions and Future Work	28
	4. Tas	sk 4. Probabilistic Degradation Model of Coated Pipe Wall Due to Excessive C	CP. 29
	4.1.	Background and Objectives in the 3 <sup>rd</sup> Annual Report Period	29
	4.2.	Research Progress in the 3 <sup>rd</sup> Annual Report Period	29
	4.3.	Conclusions	36
	4.4.	Future Work	37
	5. Tas	sk 5. Determination of Recoating Time Using Reliability-based Approach	37
	6. Tas	sk 6. Industrial Collaborations	37
Ref	erences		38

# **Section A: Business and Activities**

#### (a) Contract Activities

#### **Contract Modifications:**

The one-year no-cost extension has been requested and approved in this reporting period. The project is extended to end on September 29, 2026.

#### **Educational Activities:**

#### o Student mentoring:

Yuhan Su, a Ph.D. student in Chemical Engineering at The University of Akron, is working on the project starting the 2<sup>nd</sup> quarter of this project.

Tanner Laughorn, an undergraduate student in Corrosion Engineering at The University of Akron, worked on this project from the 5<sup>th</sup> quarter to the 7<sup>th</sup> quarter.

Abigail Murray, an undergraduate student in Corrosion Engineering at The University of Akron, worked on this project from the 5<sup>th</sup> quarter to the 11<sup>th</sup> quarter.

Brigida Zhunio Cardenas, a Ph.D. student in Civil, Construction, and Environmental Engineering at Marquette University, is working on the project starting the 7<sup>th</sup> quarter.

Xingsen Yang, a PhD student in Civil Engineering at Rutgers University, is working on the project starting the 6<sup>th</sup> quarter of this project.

#### o Student internship: NA

#### Educational activities:

The PI (Dr. Zhou) introduced the concept of cathodic protection in the undergraduate course—Introduction to Corrosion Science and Engineering at The University of Akron.

The PI (Dr. Zhou) introduced corrosion protective coatings in the undergraduate and graduate course—Corrosion Protection by Coatings at The University of Akron.

### o Career employed:

Tanner Laughorn, who worked on this project, graduated in May 2024 and started his career as a Pipeline Engineer at Burns & McDonnell.

Abigail Murray, who worked on this project, graduated in May 2025 and started her career as a Project Engineer at Marathon Petroleum Corporation.

#### o Others: NA

# Dissemination of Project Outcomes:

# Oral presentation:

Yuhan Su, Qixin Zhou, "Performance evaluation of pipeline coating disbondment under excessive cathodic protection," 2025 AMPP Annual Conference, April 6–10, 2025, Nashville, Tennessee, US.

Citations of The Publications: NA

#### Others:

On December 4, 2024, a mid-term review meeting through Microsoft Teams was conducted with participants of all three PIs and their graduate students, PHMSA personnel, James Powell and Nusnin Akter, to report on this project's progress.

On January 27, 2025, the previous program manager, Terry Powell, visited Dr. Qixin Zhou's lab at The University of Akron. The PhD student, Yuhan Su, gave a presentation about the current progress at The University of Akron. Dr. Hao Wang (co-PI) attended the meeting in person, and Dr. Qindan Huang (co-PI) and graduate students joined the meeting through Microsoft Teams. We also showed the testing facility, coating samples, vintage pipes, and experimental setups to Terry and Dr. Wang.

# (b) Financial Summary

#### Federal Cost Activities:

#### o PI/Co-PIs/students involvement:

One graduate student from The University of Akron was partially supported by this project for salary during this reporting period.

One graduate student from Rutgers University was partially supported by this project for salary during this reporting period.

One graduate student from Marquette University was partially supported by this project for salary during this reporting period.

The PI and Co-PIs were charged the summer salary from this project based on the budgeted number.

#### o Materials purchased/travel/contractual (consultants/subcontractors):

Materials were purchased for experimental measurement and testing at The University of Akron during this reporting period.

Travel support was for the graduate student, Yuhan Su, to attend the AMPP 2025 annual conference.

#### Cost Share Activities:

#### o Cost share contribution:

Cost share contribution includes graduate student tuition remission, PIs' academic salary, and indirect costs at The University of Akron, Marquette University, and Rutgers University during this reporting period.

# (c) Project Schedule Update

# Project Schedule:

The proposed research tasks and milestones updated in September 2024 are shown in Table 1. Task 1 is on the schedule and completed. Task 2 is on the schedule, and all the experiments are completed, but we would like to have two more quarters for data analysis and draft writing. Task 3 is on the schedule. Task 4 is on the schedule. Tasks 4 and 5 need the experimental data from Task 2 and simulation data from Task 3 to generate a database for calculations. It takes more time to wait for the results from Task 2 and Task 3.

**Table 1.** Schedule and milestones of proposed tasks.

Tasks	Year 1				Year 2				Year 3			
Task 1. Coating & influencing factors identification												
Task 2. Coating performance evaluation												
Task 3. Simulation of coating disbondment & CP												
Task 4. Probabilistic coating degradation model												
Task 5. Recoating time determination												
Task 6. Industrial collaborations												

#### Corrective Actions:

The updated research tasks and milestones are shown in Table 2. The orange ones are those updated, and the blue ones are those not changed.

**Table 2.** Updated schedule and milestones of proposed tasks.

Tasks		Year 1		Year 2			Year 3			Year 4					
Task 1. Coating & influencing factors identification															
Task 2. Coating performance evaluation															
Task 3. Simulation of coating disbondment & CP															
Task 4. Probabilistic coating degradation model															
Task 5. Recoating time determination															
Task 6. Industrial collaborations															

# (d) Status Update of the 12th Quarter Technical Activities

Task 1: Identification of vintage pipeline coatings and influencing factors in coating cathodic

disbondment (The University of Akron and Marquette University)

Task 1 is completed.

Task 2: Evaluation of coating cathodic disbondment considering key influencing factors through laboratory testing (The University of Akron)

The Ph.D. student, Yuhan Su, at The University of Akron, is working on this task.

The three experimental subtasks: 1) evaluation of cathodic disbondment performance in pipeline coatings, 2) the onset of degradation of pipeline coatings, and 3) the cathodic disbondment assessment of field-aged pipeline coatings, have been conducted. Their results are described in Section B.

Task 3: Numerical simulation of pipeline coating disbondment behavior and CP system (Rutgers University)

The PhD student, Xingsen Yang, at Rutgers University, is working on the COMSOL simulation this quarter.

The simulation model was compared with experimental data from Task 2 for verification. Model sensitivity was also studied for five influencing factors.

Task 4: Probabilistic degradation model of coated pipe wall due to excessive CP (Marquette University)

The PhD student, Brigida Zhunio Cardenas, at Marquette University, is working on this task this quarter.

During the reporting period, preliminary modeling has been conducted on predicting coating disbondment rate using a dataset from literature and testing data from Task 2; a database has also been established on steel corrosion rate under CP on steel, considering coating disbondment.

Task 5: Determination of recoating time using reliability-based approach (Marquette University)

Task 5 will start when Task 4 is completed.

# Section B: Detailed Technical Results in the Report Period

# 1. Task 1. Identification of Vintage Pipeline Coatings and Influencing Factors in Coating Cathodic Disbondment

Buried pipelines are protected from corrosion attack by coating and cathodic protection (CP). However, excessive CP could cause serious damage to many types of vintage pipeline coatings and, consequently, pipeline integrity.

The objective of Task 1 is to understand the conditions under which the vintage coating experiences cathodic disbondment and the key influencing factors on the cathodic disbondment. The experimental design is based on the study of the literature review and the survey from pipeline companies.

Through the literature reviews, the conditions for pipeline coatings that experience cathodic disbondment are studied and understood. The survey from pipeline companies also provides additional information on coatings and CP conditions in the field. The experimental design in Task 2 is constructed based on the study of the literature review and the survey.

Task 1 was completed in the  $2^{nd}$  year of the project. Details of the research outcomes and conclusions of Task 1 are reported in the  $2^{nd}$  Annual Report.

# 2. Task 2. Evaluation of Coating Cathodic Disbondment Considering Key Influencing Factors through Laboratory Testing

# 2.1. Background and Objectives in the 3<sup>rd</sup> Annual Report Period

A systematic coating performance evaluation was designed and conducted through experimental testing to study coating cathodic disbondment, considering key influencing factors. The objective of Task 2 in this reporting period was to perform the systematic evaluation of coating performance.

# 2.2. Research Progress in the 3<sup>rd</sup> Annual Report Period

### 2.2.1. Experimental design

The experimental design on the evaluation of coating cathodic disbondment included the selection of coating, the selection of metal, solution, CP level, and characterization method, as summarized in **Figure 1**. Each item in the experimental design is discussed below.

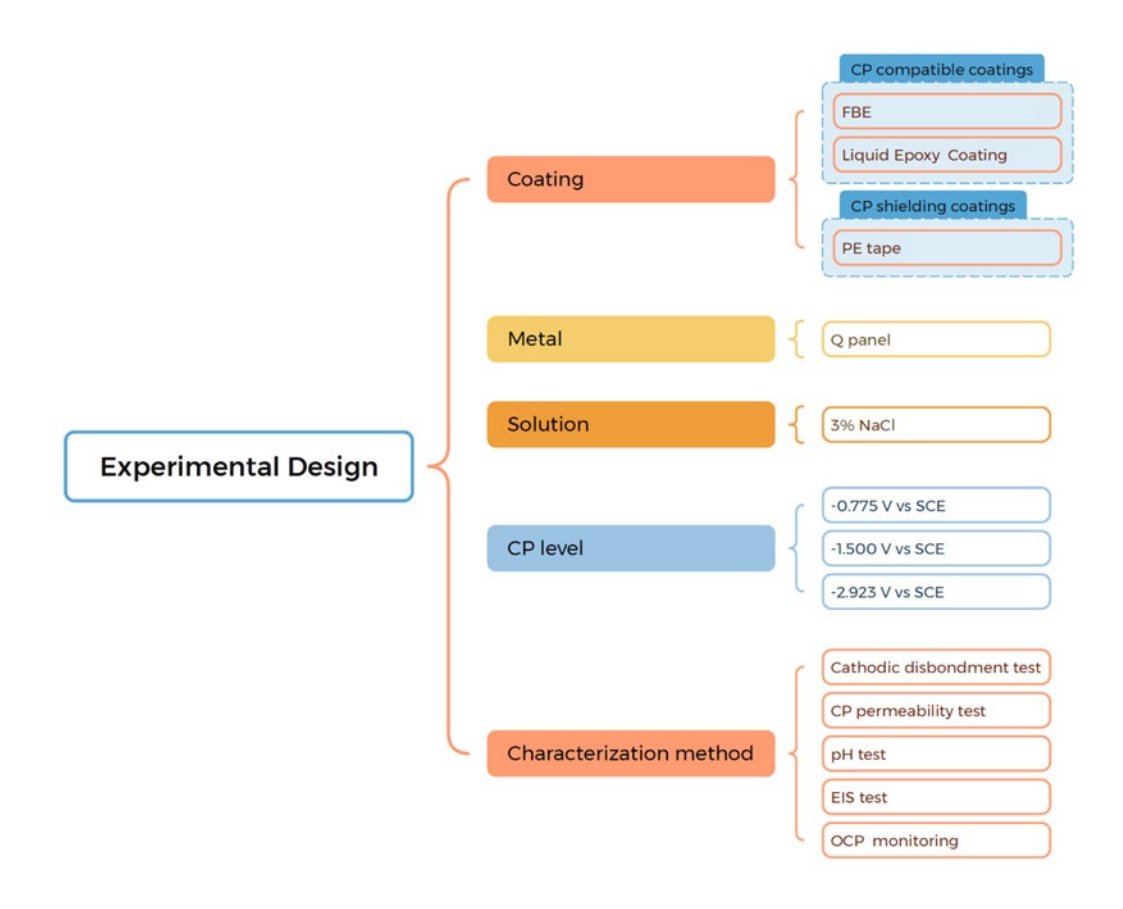


Figure 1. Experimental design for the study of coating cathodic disbondment.

## (1) Coatings and metal

Two types of CP-compatible coating were selected for the coating disbondment study in this project. A liquid epoxy coating (3M<sup>TM</sup> Scotchkote<sup>TM</sup> 323+), a two-part system designed to protect steel pipe from the harsh effects of corrosion, was used as one representative of a CP-compatible coating. The average coating thickness of this liquid epoxy coating was around 15 mil.

The second CP-compatible coating—fusion-bonded epoxy (FBE) was purchased from Midwest Coating Company. The coating samples were customized and designed to have a one-layer FBE coating with a thickness of around 15 mil on a Q-panel substrate. The FBE coating samples were divided into two categories: coating with defects and coating without defects, based on their initial electrochemical impedance modulus tested by electrochemical impedance spectroscopy (EIS).

The polyethylene/butyl rubber pipeline tape (PE tape) coating was purchased from Starlight Maintenance, Inc., and applied in the lab. The coating had a similar thickness of 15 mil.

The Q panel (S36) was chosen as the substrate for the coatings because S36 panels are produced to have excellent chemical resistance, weathering, corrosion resistance, and physical properties. Thus, the S36 Q panel is commonly used as a metal substrate for corrosion protective coatings.

# (2) Solution

A 3 wt.% NaCl solution was selected as the testing medium according to ASTM G8, ASTM G95, and NACE TM0015 standards. The solution was prepared by adding NaCl solids to the deionized water. The pH of the 3 wt.% NaCl solution was around 6.

# (3) <u>Initial disbondment diameter</u>

The initial disbondment was artificially made by drilling a hole in the coating surface, as specified by the standards. The fully cured coating panel was drilled in the middle of the surface to get a hole around 3.2 mm (0.125 in) in diameter, based on ASTM G95. The exposed area was then cleaned with isopropyl alcohol and blown with air to dry. The exact diameter and the exposed area were measured by using an OLYMPUS stand scope. An example of these coating samples with the artificial hole is shown in **Figure 2**.

# (4) Cathodic protection conditions

The cathodic potentials used for coatings in this cathodic disbondment study were -0.775, -1.5, and -2.923 V vs. SCE. The three CP potentials are the representatives of the standard value of CP, the medium value of CP, and the high value of CP to cover the used CP potential range, including the reported over-protection level. The coating samples were exposed to the CP conditions under different durations (1d, 7d, 14d, 21d, and 28d). This duration included short-term and long-term periods to provide a systematic study.

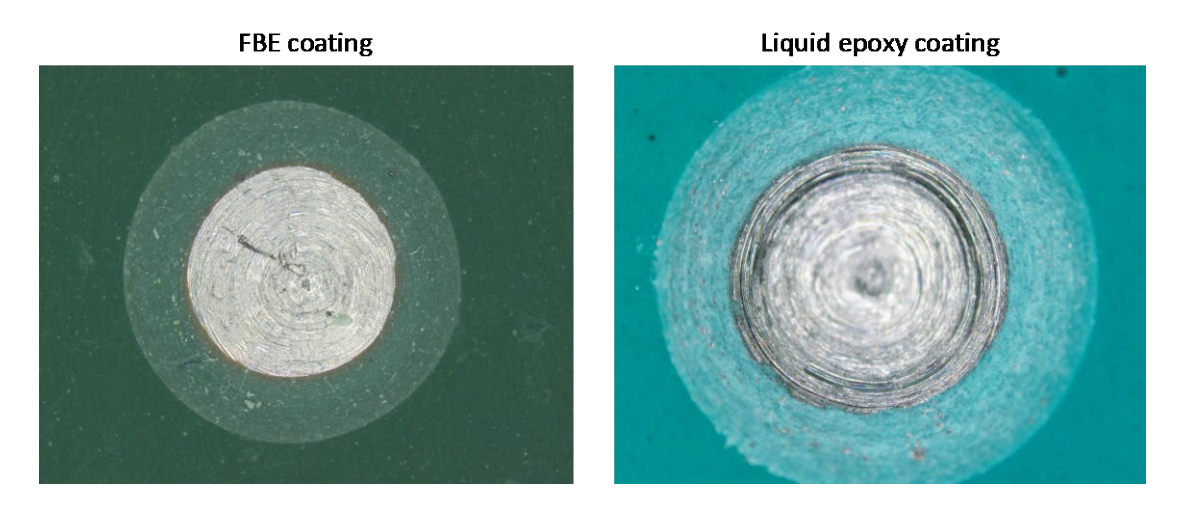


**Figure 2.** Coating samples with an artificial hole of FBE coating and liquid epoxy coating.

#### (5) Coating characterization

The experimental setups for applying CP while monitoring coating disbondment behavior have been designed and used for the testing, as shown in **Figure 3**. The open circuit potential was measured before and after the cathodic disbondment test. Besides, the electrochemical impedance spectroscopy (EIS) was performed before and after the test. The local pH around the disbondment area was measured by a micro pH meter. The disbonded area of the coating surface was characterized by optical microscopy and analyzed using ImageJ software. Blisters or rusts were

visually inspected and recorded, followed by a cathodic disbondment test.

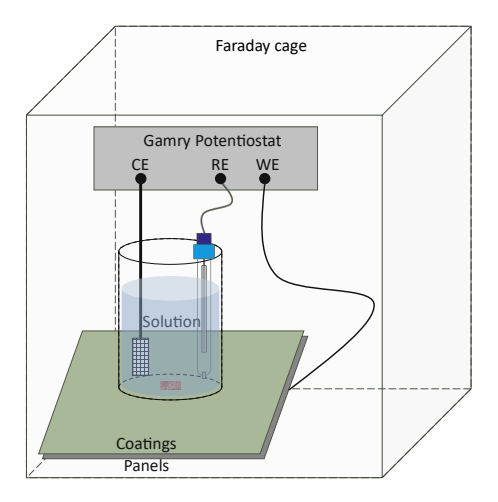


**Figure 3.** The electrochemical cell for the coating cathodic disbondment test. S-type Q-panel works as a working electrode (WE), a saturated calomel electrode as a reference electrode (RE), and a platinum sheet as a counter electrode (CE).

## 2.2.2. Experimental protocol for the study of coating cathodic disbondment

The experimental testing protocol was designed to study the coating cathodic disbondment, as illustrated in **Figure 4**. The fully cured coating panel was measured for thickness. Then, an artificial defect was performed according to ASTM G95 to generate a holiday with 0.125 inches in diameter. The coating surface was captured for its initial image. Next, the electrochemical cell was filled with a 3 wt.% NaCl solution. The pH of the solution, as well as the initial electrochemical impedance of the coating sample, was measured. After the EIS test, an open circuit potential (OCP) was measured and run for 30 minutes. Then, the cathodic protection was applied to the coating sample through a Potentiostat. After applying cathodic protection for the designed time, the electrochemical cell (coating sample) was tested for its OCP for 30 minutes to several hours until it reached a stable potential. Also, the pH near the disbonded area after cathodic protection was monitored, as well as the EIS measurement. Finally, the coating sample was removed from the test cell. The coating cathodic disbondment area was analyzed using ImageJ software. Blisters or rust on the coating surface were inspected and recorded, and the image of the coating was captured.

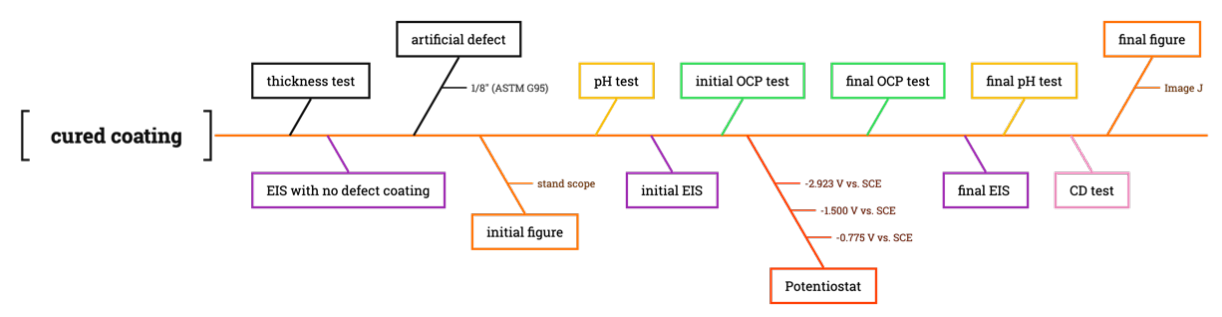


**Figure 4.** Experimental protocol for the study of coating cathodic disbondment.

The coating cathodic disbondment testing procedure is illustrated in **Figure 5**. It includes the experimental setup for the electrochemical cell, CP potential conditions, and how to identify the disbonded area after the cathodic disbondment test.

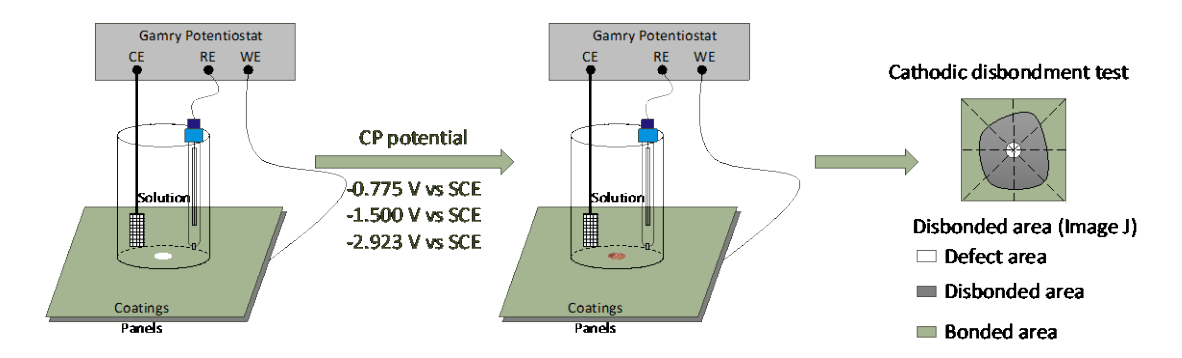


**Figure 5.** Coating cathodic disbondment testing procedure.

#### 2.2.3. Results

# (1) Morphology

**Figure 6** presents the surface morphologies of steel substrates coated with different coatings, following 7-day cathodic disbondment (CD) testing under various CP potentials. For FBE coatings and liquid epoxy coatings, when the CP potential was -0.775 V vs SCE, the CD area was not that big, indicating a good adhesion between the coating and the metal substrate. As the CP potential shifted to more negative values (-1.500V and -2.923V vs SCE) over the threshold of the overprotection, the CD areas became bigger. However, it is worth noting that for the PE tape coating, no obvious trend in the coating CD area was observed. By contrast, as the CP potential shifted to more negative values, the corrosion products formed on the metal surface at the initial defect site showed a growing trend. Notably, this phenomenon was not limited to the 7-day testing duration but also persisted in tests with longer durations, as shown in **Figure 7**.

#### (2) Coating disbondment

**Figure 8** shows the cathodic disbondment area of three coatings, liquid epoxy coatings (triangle), FBE coatings (circle), and PE tape coatings (rectangular), under different time durations and CP potentials. The ordinate represents the cathodic disbondment area in a unit of cm<sup>2</sup>, and the abscissa represents the time duration. Three CP potential conditions under investigation were –0.775 V vs. SCE (blue), –1.500 V vs. SCE (red), and –2.923 V vs. SCE (green).

**Figure 8(a)** shows the relationship between the cathodic disbondment (CD) area of liquid epoxy coatings and time duration under three different CP potentials. The more negative CP potentials, the CD area exhibited a clear increasing trend with extended time duration. Notably, the –2.923 V vs SCE condition led to a more rapid and substantial growth of the CD area, highlighting the significant impact of overly negative CP potentials on accelerating cathodic disbondment of liquid epoxy coatings.

Figure 8(b) shows the relationship between the CD area of FBE coatings and time duration under

different CP potentials. When the CP potential was -0.775 V vs. SCE, the CD area of FBE coatings remained nearly constant and close to 0 cm<sup>2</sup> throughout the whole test period of 30 days. For the CP potential of -1.500 V vs. SCE, the CD area showed a gradually increasing trend with time. When the CP potential was negative to -2.923 V vs. SCE, the CD area initially rose sharply within the first 5 days, reached a peak, and then exhibited a fluctuating yet relatively high level as time progressed. This plot indicates that more negative CP potentials (especially -2.923 V vs SCE) can significantly accelerate the cathodic disbondment process of FBE coatings.

**Figure 8(c)** illustrates the relationship between the CD area of PE coatings and time duration under varying CP potentials. As depicted, the CD area fluctuated over time. The differences in CD area among the three potentials across different time durations were relatively indistinct. Therefore, the cathodic disbondment of the PE coatings didn't show a clear correlation with the CP potential.

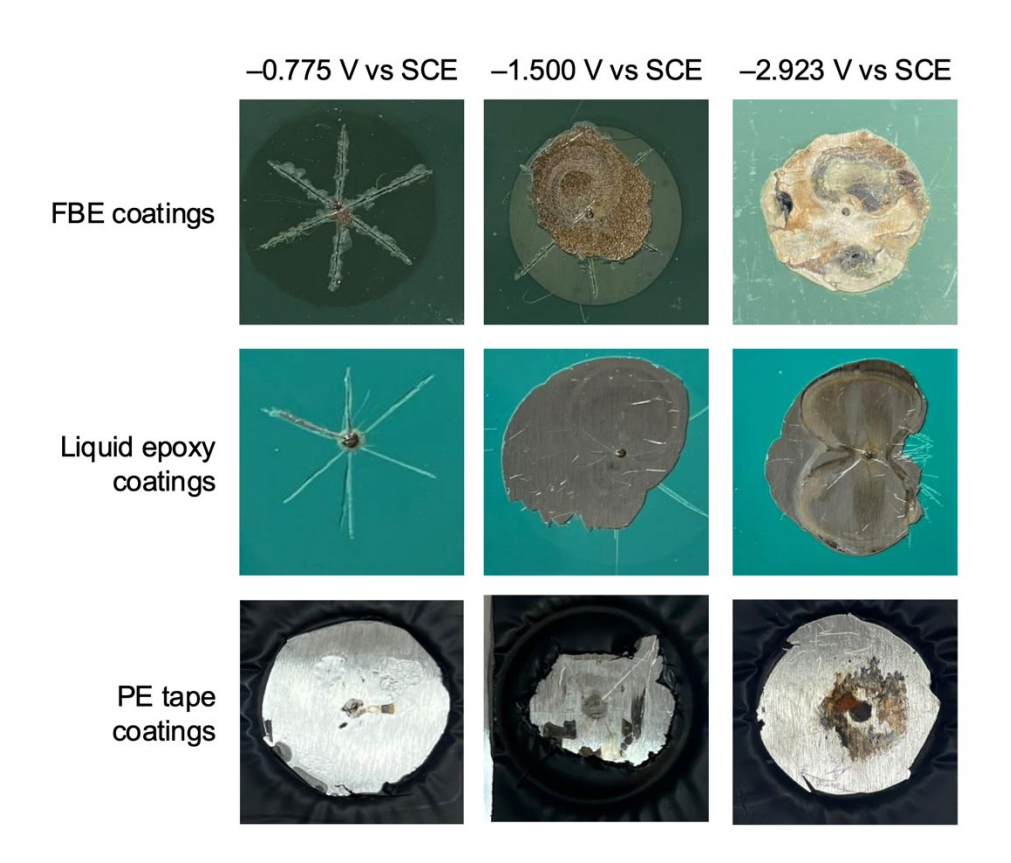


**Figure 6.** Diagram of the cathodic disbondment morphology of FBE coatings, liquid epoxy coatings, and PE coatings under different CP potential conditions of –0.775 V, –1.500 V, and – 2.923 V vs SCE for 7 days.

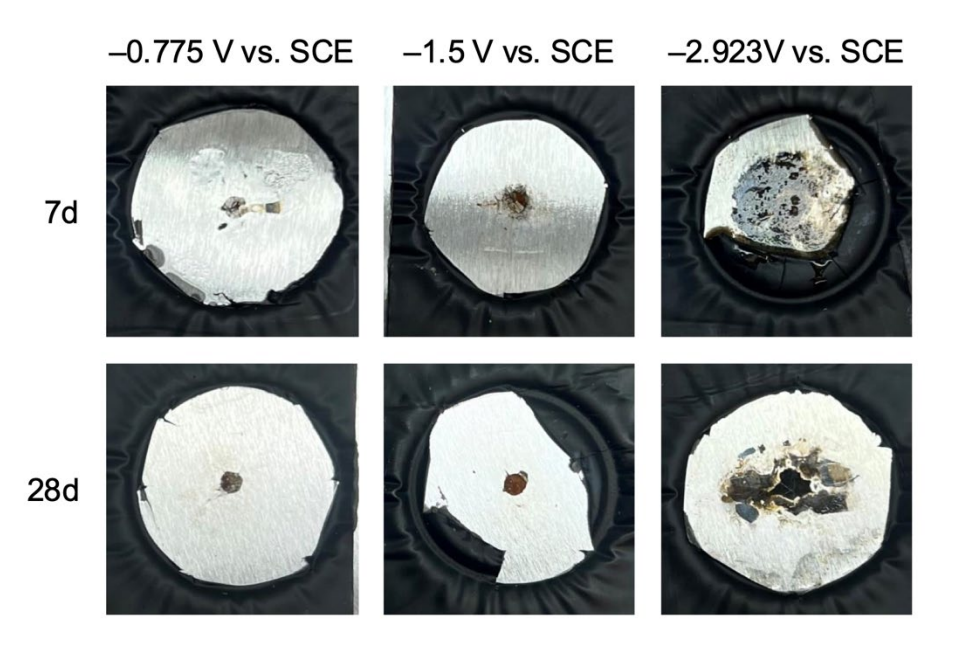


**Figure 7.** Diagram of the cathodic disbondment morphology of PE coatings under different CP potential conditions of -0.775 V, -1.500 V, and -2.923 V vs SCE for 7 days and 28 days.

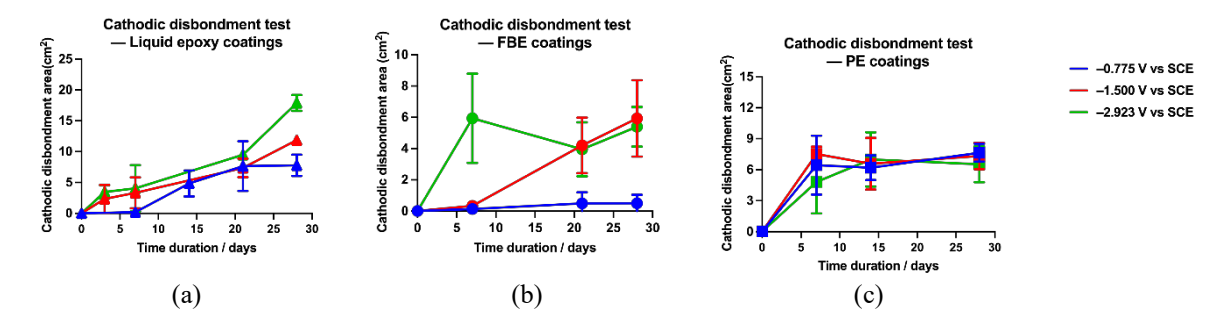


**Figure 8.** The cathodic disbondment area of three different coating systems under three different CP potentials over time: (a) liquid epoxy coatings, (b) FBE coatings, and (c) PE coatings.

To better understand the effect of CP potential on cathodic disbondment, Figure 9 shows the cathodic disbondment rate of three coating systems as a function of CP potential. The cathodic disbondment rate refers to the cathodic disbondment area divided by time. For FBE coatings, the cathodic disbondment rate showed a gradual increase with more negative CP potentials. Liquid epoxy coatings exhibited a more pronounced rising trend in disbondment rate as the CP potential became more negative. In contrast, the PE coatings showed a relatively stable disbondment rate, with minimal variation across different CP potentials. These results highlighted the divergent responses of coating systems to CP potential: liquid epoxy coatings and FBE coatings were more susceptible to accelerated cathodic disbondment under increasingly negative CP conditions, whereas the cathodic disbondment of PE coatings didn't have a clear correlation with the CP potential. The differentiation underscored the importance of tailoring CP strategies to the specific

coating type to mitigate cathodic disbondment.

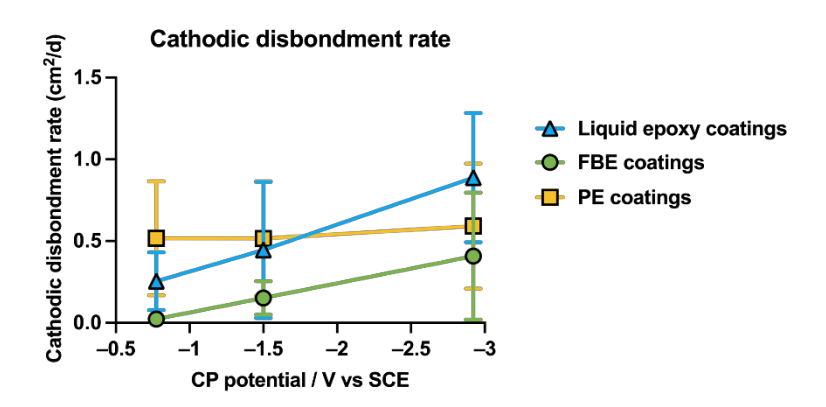


**Figure 9.** The cathodic disbondment rate of the three coatings under three CP potentials.

# (3) Solution alkalinity

**Figure 10** shows the final solution pH around the cathodic disbondment area of three coatings, liquid epoxy coatings (triangle), FBE coatings (circle), and PE tape coatings (rectangular) under different time durations and CP potentials. The ordinate represents the pH value at the position around the artificial defect, and the abscissa represents the time duration. Three CP potential conditions under investigation were –0.775 V vs. SCE (blue), –1.500 V vs. SCE (red), and –2.923 V vs. SCE (green).

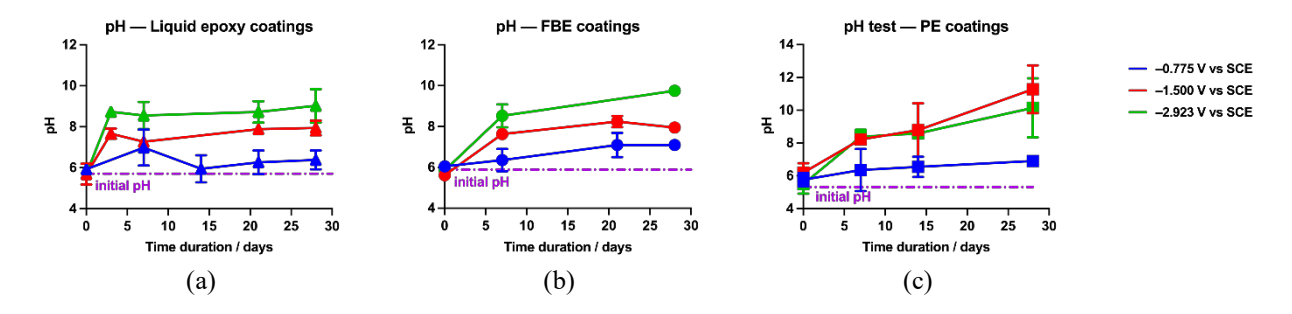


**Figure 10.** The final solution pH near the coating disbondment area of three different coating systems under three different CP potentials over time: (a) liquid epoxy coatings, (b) FBE coatings, and (c) PE coatings.

**Figure 10(a)** illustrates the final solution pH of liquid epoxy coatings over a 30-day duration under three CP potentials. The initial solution pH is shown as a purple dashed line. The final pH was higher than the initial pH, regardless of the applied CP potential. Under -0.775 V vs. SCE condition, pH remained relatively stable over time. For the CP potential of -1.500 V vs. SCE, pH rose steadily in the first 5 days, then stabilized at around 8. When the CP potential was negative to -2.923 V vs. SCE, the pH increased to around 9 within 5 days, followed by a sustained increase to around 10 at 30 days. These trends indicate that more negative CP potential accelerated the alkaline environment at the coating-metal interface, corresponding to the cathodic reaction.

Figure 10(b) illustrates the pH change of FBE coatings across 30 days under three different CP

potentials. The initial solution pH is denoted by a purple dashed line, which was around 6. Evidently, the final pH was also higher than the initial pH. At –0.775 V vs. SCE, pH remained nearly constant. When the CP potential was –1.500 V vs. SCE, pH increased to around 8 within 10 days and stabilized. The CP potential of –2.923 V vs. SCE induced a steeper pH increase, reaching 9 within 5 days and continuing to climb to approximately 10 by 30 days. This data aligns with that presented in **Figure 10(a)**, confirming that negative CP potentials promoted an alkaline environment at the interface between the coating and metal.

**Figure 10(c)** presents the pH change of PE coatings over 30 days under different CP potentials. Consistent with observations in liquid epoxy coatings and FBE coatings, the final pH values across all test conditions were higher than the initial pH, indicating an alkaline environment developed at coating—metal interfaces when applying CP. When the CP potential was –0.775 V vs. SCE, the pH remained stable at approximately 6 throughout the test duration. For CP potential of –1.500 V vs. SCE and –2.923 V vs. SCE, the pH exhibited a time-dependent increasing trend. The consistency pH increase for all the coating systems indicates a clear correlation between CP potential and environmental alkalinity: the more negative the CP potential, the more pronounced the alkaline environment at the metal-coating interface.

# (4) Open circuit potential

The open circuit potential (OCP), also referred to as the corrosion potential, could indicate how susceptible a material is to corrosion [1, 2]. Furthermore, OCP can be used to analyze the barrier, coatings, and corrosive environments. The increase of OCP could indicate multiple protective mechanisms, including the protective layer formation, the addition of cathodic inhibitors to the corrosive medium, or the effective barrier action of the coating against corrosive agent penetration to the metal surface [2].

**Figure 11** shows the OCP after different duration times (final OCP) of the disbonded coating samples for the three coatings: liquid epoxy coatings (triangle), FBE coatings (circle), and PE tape coatings (rectangular) under different time durations and CP potential, respectively. The ordinate represents the final OCP value in mV vs. SCE, and the abscissa represents the time duration. Three CP potential conditions under investigation were –0.775 V vs. SCE (green), –1.500 V vs. SCE (blue), and –2.923 V vs. SCE (yellow).

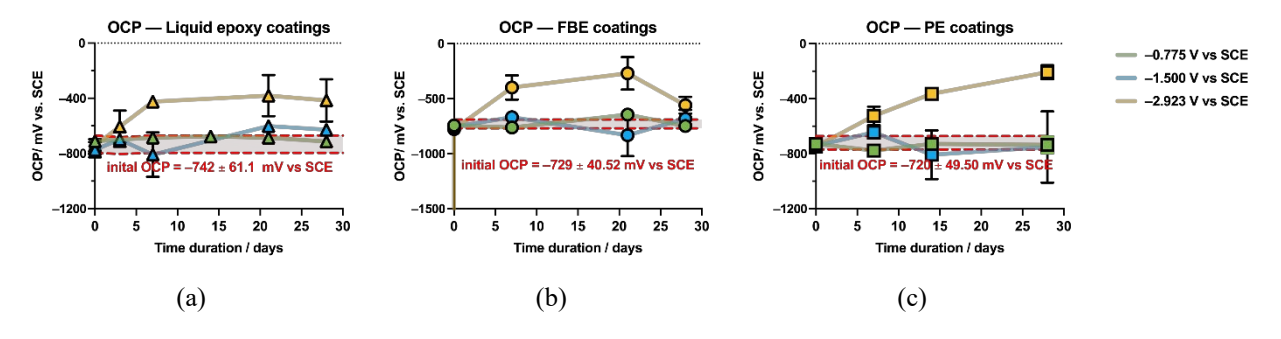


**Figure 11.** The final OCP of three different coating systems under three different CP potentials over time: (a) liquid epoxy coatings, (b) FBE coatings, and (c) PE coatings.

**Figure 11(a)** illustrates the final OCP change of disbonded coating samples with liquid epoxy coatings under three CP potentials. The initial OCP, indicated by the red dashed band, was around −0.742±0.06 V vs. SCE. When the applied CP potentials were −0.775 V vs. SCE and −1.500 V vs. SCE, the final OCP remained within the initial OCP range throughout the time. In contrast, the final OCP under the CP potential of −2.923 V vs. SCE showed a distinct upward trend, significantly exceeding the initial OCP range.

**Figure 11(b)** shows the final OCP change of disbonded FBE coating samples over 30 days under three CP potentials. The initial OCP, marked by the red dashed band, was around  $-0.729\pm0.04$  V vs. SCE. For CP potential of -0.775 V vs. SCE and -1.500 V vs. SCE, the final OCP stayed within the initial OCP range. However, when the CP potential was negative to -2.923 V vs. SCE, the final OCP increased notably beyond this range.

**Figure 11(c)** presents the final OCP change of disbonded PE coating samples under three CP potentials. The initial OCP, shown by the red dashed band, was around −0.720±0.05 V vs. SCE. For CP potential of −0.775 V vs. SCE and −1.500 V vs. SCE, the final OCP values fluctuated within the initial OCP range, showing minimal deviation from the baseline. Conversely, when the CP potential was negative to −2.923 V vs. SCE, the final OCP rose distinctly above this initial range.

The three coatings all demonstrate that the more negative CP potential drove the OCP to a more positive state. A highly negative CP potential could accelerate the formation of corrosion products, which is corroborated by morphological observations in **Figure 6**. These corrosion products likely act as a barrier, inhibiting oxygen diffusion to the metal surface and thereby inducing a positive shift in the OCP [3].

#### 2.3. Conclusions

The experimental setups and testing procedures for the study of coating cathodic disbondment have been designed and established. A systematic study of coating cathodic disbondment has been conducted. Three different coatings, three different CP potentials, and different duration times were investigated. The coating cathodic disbondment has been evaluated by cathodic disbondment area, pH near the disbonded area, OCP, and surface morphology.

Both CP-compatible coatings showed increased cathodic disbondment area as the applied CP potential became more negative. However, the CP-shielding coating didn't present a clear correlation between the cathodic disbondment and the CP potential. All coating systems showed the development of an alkaline environment at the disbonded area, which demonstrates the accumulation of hydroxyl groups from cathodic reaction under CP conditions. The positive shift of OCP under the more negative CP potential was a result of the accelerated accumulation of corrosion products generated at the disbonded area.

So far, based on experimental outcomes, guidance is needed to match CP potential with different coating systems. Specifically, for CP-compatible coatings, a stricter control of the applied CP is necessary to avoid over-protection that exacerbates the coating cathodic disbondment, while for CP-shielding coatings, which are not sensitive to CP potential, a relatively flexible CP range could be applied.

# 2.4. Future Work

The initiation of coating cathodic disbondment will continue to be studied. It is expected to know the initiation mechanisms for different coatings under excessive CP potentials. The data analysis will be finished next year, and one manuscript will be constructed and submitted for a journal publication.

## 3. Task 3. Numerical Simulation of Pipeline Coating Disbondment Behavior and CP System

# 3.1. Background and Objectives in the 3<sup>rd</sup> Annual Report Period

CP safeguards steel pipelines by applying an electric current, thereby effectively preventing corrosion. According to the developmental mechanism of cathodic disbondment (CD), CD is often initiated by the formation of holidays caused by accidental coating damage, indicating that coating delamination typically occurs after the formation of holidays. Meanwhile, once disbondment forms, holidays serve as channels and pathways for CP current flow and particle exchange. Therefore, integrating holidays and disbondment into a model is essential for accurately modeling CD scenarios, enabling a more precise investigation of the electrochemical processes within the CD system and evaluation of the effectiveness of CP.

In this task, a numerical model integrating coating holiday and disbondment was established to investigate corrosion on pipeline surfaces under the influence of CP, as well as to analyze particle exchange and distribution within the system. Given that pH is a critical factor influencing the progression of disbondment based on experimental studies in the literature, the analysis will be conducted to investigate the effects of various influencing factors on pH distribution.

# 3.2. Research Progress in the 3<sup>rd</sup> Annual Report Period

## 3.2.1. Model setups

# (1) Model geometry

The schematic representation of the crevice geometry employed in the model proposed in this study is illustrated in **Figure 12**. The system is symmetric about the line OY, and the analysis focuses on this symmetric cross-section. The domain of the disbonded coating system (OABCDEFG) is partitioned into two regions: the holiday (OABCDG) and the disbondment (DEFG). The boundaries of the system include the symmetry line OB, the metal surface OF, and the coating sections CD, DE, and EF, as well as the holiday opening BC.

To simplify the model calculations, the following assumptions are considered:

- 1. The disbondment is simplified to a narrow rectangular shape, and the parts of the pipeline with well-adhered coating are excluded from the system. It is assumed that the coating is impermeable to both current and oxygen. During cathodic protection of the metal surface within the disbonded coating system, current flows through the electrolyte within the holiday and disbondment to reach the metal surfaces.
- 2. Concentration gradients are considered negligible at distances far from the metal surface. This assumption introduces a boundary known as the bulk boundary, where both species concentration and potential are held constant. In this model, the bulk boundary is defined at the opening of the holiday.
- 3. The crevice is initially filled with a neutral sodium chloride electrolyte with minimal ferrous content, and the bulk solution outside the holiday is assumed to be saturated with oxygen from the

air at 25°C and 101.3 kPa. Homogeneous reactions were not considered in this analysis.

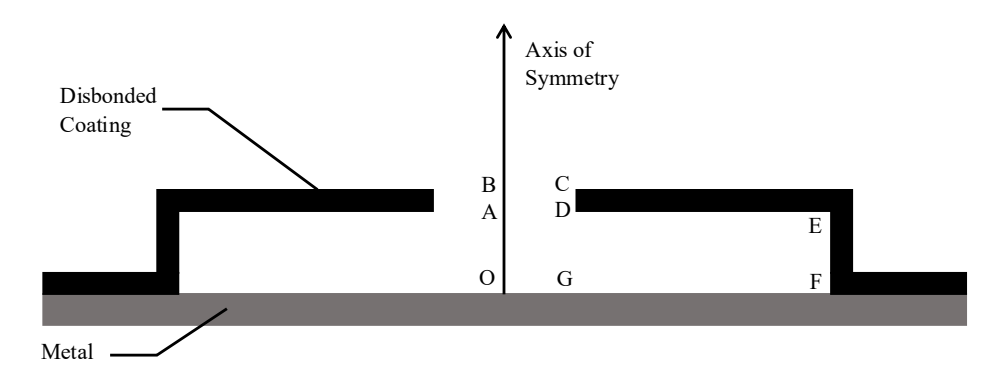


Figure 12. Schematic diagram of the simulation domain.

#### (2) General transport equations

In dilute electrochemical systems, the steady-state mass conservation equation governs the concentration of each species  $c_i$ :

$$0 = -\nabla \cdot N_i + R_i \tag{1}$$

where  $N_i$  is the net flux of species i and  $R_i$  is the rate of production or depletion of species i by chemical reactions, which can be given by

$$R_i = \frac{i_{net}}{nF} \tag{2}$$

where  $i_{net}$  is the current density of the reaction; n is the number of charges transferred in the reaction; and F is Faraday's constant (96500 C/mol).

The term of flux  $N_i$  in **Equation 1** is given by the Nernst-Planck equation, which consists of contributions from migration, diffusion, and convection:

$$N_i = -z_i u_i c_i F \nabla \Phi - D_i \nabla c_i + c_i v \tag{3}$$

where  $c_i$  is the concentration of species i;  $\Phi$  is the local electrolyte potential;  $z_i$  is the ionic charge number of species i;  $u_i$  is the mobility;  $D_i$  is the diffusion coefficient; and v is the convection velocity of the electrolyte.

Under the assumption that the electrolyte is stagnant, the term of convection is negligible, **Equation 3** is recast as:

$$N_i = -z_i u_i c_i F \nabla \Phi - D_i \nabla c_i \tag{4}$$

The term for mobility  $u_i$  can be rewritten using the Nernst-Einstein equation as follows:

$$u_i = \frac{D_i}{RT} \tag{5}$$

where R is the molar gas constant (8.314 J/(mol·K)) and T is the absolute temperature (298K).

By combining Equations 1, 2, 4, and 5, the general steady-state governing equation for species transport is obtained:

$$0 = \frac{z_i F}{RT} D_i \left( \frac{\partial c_i}{\partial x} \frac{\partial \Phi}{\partial x} + c_i \frac{\partial^2 \Phi}{\partial x^2} \right) + D_i \frac{\partial^2 c_i}{\partial x^2} + \frac{i_{net}}{nF}$$
 (6)

# (3) Electrochemical kinetic equations

Electrochemical reactions occur at the surface of the pipeline, including both anode metal dissolution and cathodic reactions, which encompass oxygen reduction and hydrogen evolution:

Anode:  $Fe \rightarrow Fe^{2+} + 2e^{-}$ 

Cathode:  $O_2 + 2H_2O + 4e^- \rightarrow 4OH^-$ 

$$2H_2O + 2e^- \rightarrow 2OH^- + H_2$$

The Tafel equations are applied for different reactions:

$$i_{Fe} = i_{Fe}^{0} \times 10^{\frac{\eta_{Fe}}{A_{Fe}}} \tag{7}$$

$$i_{O_2} = \frac{c_{O_2}}{c_{O_2}^{ref}} \times i_{O_2}^0 \times 10^{\frac{\eta_{O_2}}{A_{O_2}}}$$
(8)

$$i_{H_2} = i_{H_2}^0 \times 10^{\frac{\eta_{H_2}}{A_{H_2}}} \tag{9}$$

where,  $i_{Fe}^0$ ,  $i_{O_2}^0$  and  $i_{H_2}^0$  are the exchange current densities for the anodic and cathodic reactions,  $c_{O2}$  is the concentration of the diffusing oxygen at the pipe level,  $c_{O_2}^{ref}$  is the reference oxygen concentration at bulk electrolyte,  $A_{Fe}$ ,  $A_{O2}$ , and  $A_{H2}$  are the anodic and cathodic Tafel slopes. The  $\eta_{Fe}$ ,  $\eta_{O_2}$ , and  $\eta_{H_2}$  are the anodic and cathodic over-potentials.

# (4) Boundary conditions

According to the assumption, the bulk boundary is positioned at the opening of the holiday. At this boundary, specifically at the mouth of the holiday (BC), the values of  $c_i$  and  $\Phi$  are set to their respective bulk conditions,  $c_{i,\infty}$  and  $\Phi_{\infty}$ , and are maintained as constant. A solution potential of  $\Phi_{\infty}=0$  was chosen, establishing a reference zero for the  $\Phi$  values calculated within the model at

the bulk boundary.

Natural boundary conditions were employed for  $c_{\text{Na+}}$ ,  $c_{\text{Cl-}}$ ,  $c_{\text{OH-}}$ , and  $c_{\text{Fe+2}}$  at all boundaries except at the mouth. At the boundaries associated with the coating (CD, DE, and EF) and the line of symmetry AB, a no-flux condition was imposed, defined by

$$N_i \cdot n = 0 \tag{10}$$

where n was the unit vector normal to the surface.

# 3.2.2. Methods of solving the model

The equations described in the model consist of second-order nonlinear partial differential equations and algebraic equations. Due to the coupling between species concentration  $c_i$  and potential  $\Phi$ , analytical solutions are not feasible, necessitating numerical methods for solution. Typically, the Finite Difference Method (FDM) is used for such purposes. This process involves applying dimensionless transformations to the equations and their associated initial and boundary conditions, followed by setting up spatial and temporal grids. Numerical iterative techniques are then employed to solve the equations. In this study, the commercial finite element software COMSOL 6.2 will be used to perform numerical simulations. The parameters used for this simulation are detailed in Table 3.

**Table 3.** The parameters used in the model.

Symbol	Values	Expression
$r_h(cm)$	0.25	Holiday radius
$r_d$ (cm)	1.0	Disbondment length
_g (cm)	0.05	Disbondment gap
$D_{\mathrm{Na^{+}}}$ (cm <sup>2</sup> /s)	1.334×10 <sup>5</sup>	Diffusion coefficient of Na <sup>+</sup>
$D_{\text{Cl-}}(\text{cm}^2/\text{s})$	$2.034 \times 10^{5}$	Diffusion coefficient of Cl <sup>-</sup>
$D_{\mathrm{OH-}}(\mathrm{cm}^2/\mathrm{s})$	$5.246 \times 10^5$	Diffusion coefficient of OH
$D_{\mathrm{Fe2^+}}(\mathrm{cm^2/s})$	$0.712 \times 10^5$	Diffusion coefficient of Fe <sup>2+</sup>
$D_{\rm O2}({ m cm^2/s})$	$2.781 \times 10^{5}$	Diffusion coefficient of O <sub>2</sub>
$c_{\mathrm{Na}^{+},\infty}(\mathrm{mol/L})$	$10^{-3}$	Concentration of Na <sup>+</sup> in the bulk solution
$c_{\text{Cl-},\infty}(\text{mol/L})$	10-3	Concentration of Cl <sup>-</sup> in the bulk solution
$c_{\mathrm{OH-},\infty}(\mathrm{mol/L})$	10 <sup>-7</sup>	Concentration of OH <sup>-</sup> in the bulk solution
$c_{\text{Fe2+},\infty}(\text{mol/L})$	10 <sup>-15</sup>	Concentration of Fe <sup>2+</sup> in the bulk solution
$c_{{\rm O2},\infty}({ m mol/L})$	2.7×10 <sup>-4</sup>	Concentration of dissolved oxygen in the
		bulk solution
$\eta_{ ext{Fe}}( ext{V})$	-0.76	Standard potential of the metal dissolution
		reaction
$i_{\rm Fe}^0  ({\rm A/m^2})$	$7.1 \times 10^{-5}$	Exchange current density of the metal
		dissolution reaction
$A_{Fe}$ (V/decade)	0.06	Tafel slope of the metal dissolution reaction

$\eta_{02}(V)$	0.189	Standard potential of the oxygen reduction reaction
$i_{O_2}^0 \text{ (A/m}^2)$	7.7×10 <sup>-7</sup>	Exchange current density of the oxygen reduction reaction
A <sub>O2</sub> (V/decade)	-0.12	Tafel slope of the oxygen reduction reaction
$\eta_{ ext{H2}}( ext{V})$	-1.03	Standard potential of the hydrogen evolution reaction
$i_{\rm H_2}^0  \left( {\rm A/m^2} \right)$	1.1×10 <sup>-2</sup>	Exchange current density of the hydrogen evolution reaction
A <sub>H2</sub>	-0.15	Tafel slope of the hydrogen evolution reaction

#### 3.2.3. Model verification

To validate the model accuracy, experimental data from Task 2 were used. For part of the Task 2 coupons, direct current (DC) measurements were taken before performing destructive tests to determine the disbondment area. This provided paired datasets of disbondment size and the corresponding DC current under various exposure durations, applied potentials, and coating materials. These data sets were subsequently employed to verify the predictive capability of the numerical model.

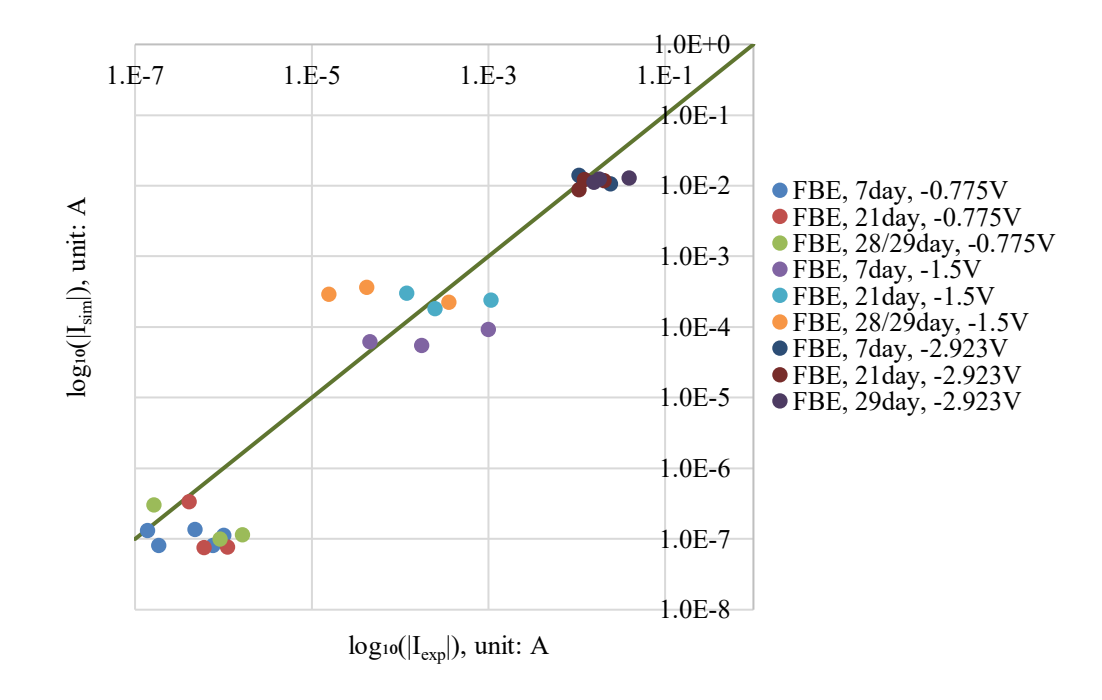
Numerical simulations were conducted using the experimentally measured disbondment areas as geometric input. For each selected case, the disbonded region was idealized as a circular area. This assumption enabled the model to be simplified to a one-dimensional radial domain extending outward from the center of the holiday.

The total current density distribution along the radial direction was calculated for all tested conditions based on their corresponding disbondment areas. The simulated total DC current  $I_{\text{sim}}$  area was obtained by integrating the radially distributed current density j(r) over the circular disbonded area using the following **Equation 11**:

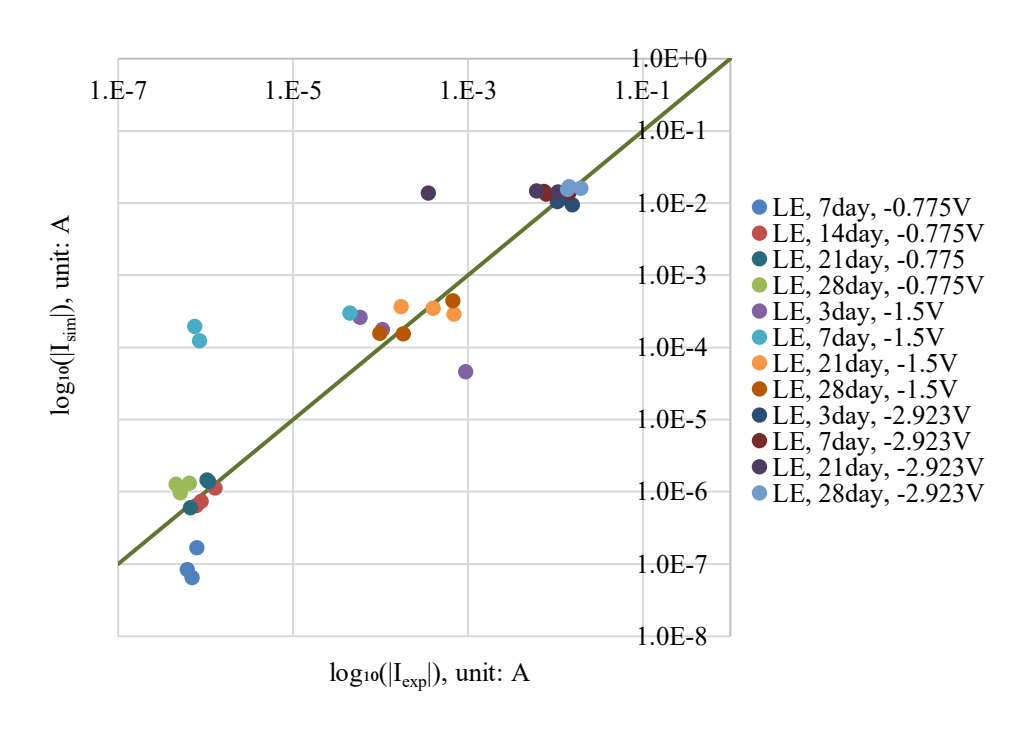
$$I_{sim} = \int_0^R j(r) \cdot 2\pi r dr \qquad (11)$$

where R was the radius of the disbonded region, calculated from the experimentally measured area.

**Figure 13** shows the comparison between simulated and experimental DC current values, plotted as the logarithm of their absolute values to accommodate the wide range of magnitudes. The data points cluster closely around the 1:1 reference line, indicating strong agreement between the model and experiments. Only the -1.5 V group shows some deviation from the 1:1 reference line, while the predictions for other applied potentials remain within an acceptable error range, suggesting the model captures the electrochemical behavior under varying coating types, CP levels, and immersion times.



(a)



(b)

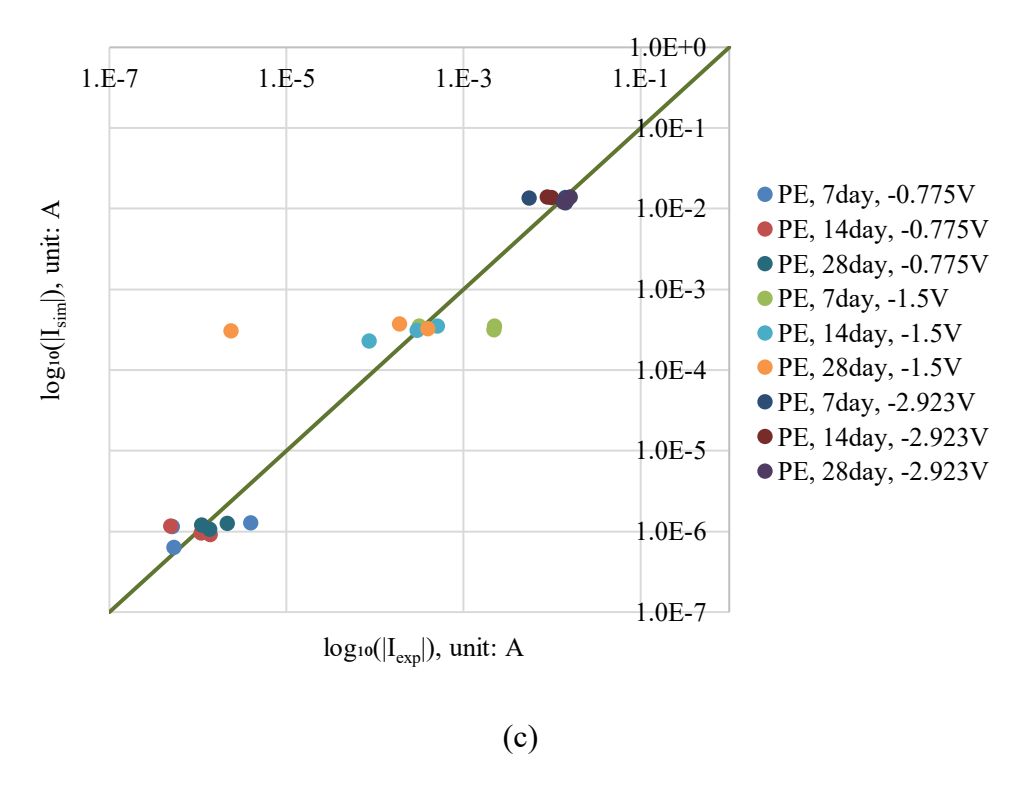


**Figure 13.** Comparison between simulated and experimental DC current for different coatings under different CP potentials and exposure durations: (a) FBE, (b) Liquid Epoxy, (c) PE.

# 3.2.4. Sensitivity analysis

After validating the numerical model against experimental DC current measurements and confirming its predictive capability across coatings and CP levels, a sensitivity analysis was conducted to systematically evaluate the influence of key geometric and environmental parameters on model outputs. To comprehensively assess the effects of various factors on cathodic disbondment, five factors were considered: applied CP potential, disbondment length, disbondment gap, soil resistivity, and oxygen concentration. Corrosion current density and local pH distribution were analyzed as key outputs.

## (1) Applied CP potential

CP reduces pipeline corrosion by shifting the steel potential to a more negative value and suppressing anodic dissolution. **Figure 14** shows the effect of applied CP potential on corrosion current density and pH distribution. Overall, more negative CP potentials markedly lower corrosion current density, indicating stronger protection. However, the current density still increases with distance into the crevice, especially under highly negative potentials, reflecting decreasing CP effectiveness in the deeper disbonded region. The difference between the holiday and disbondment areas becomes more pronounced as CP potential becomes more negative. Local pH also rises with increasingly negative CP, mainly in the disbonded area, due to intensified cathodic reactions generating hydroxide ions. This stronger alkalinity may accelerate coating disbondment despite the reduced corrosion current.

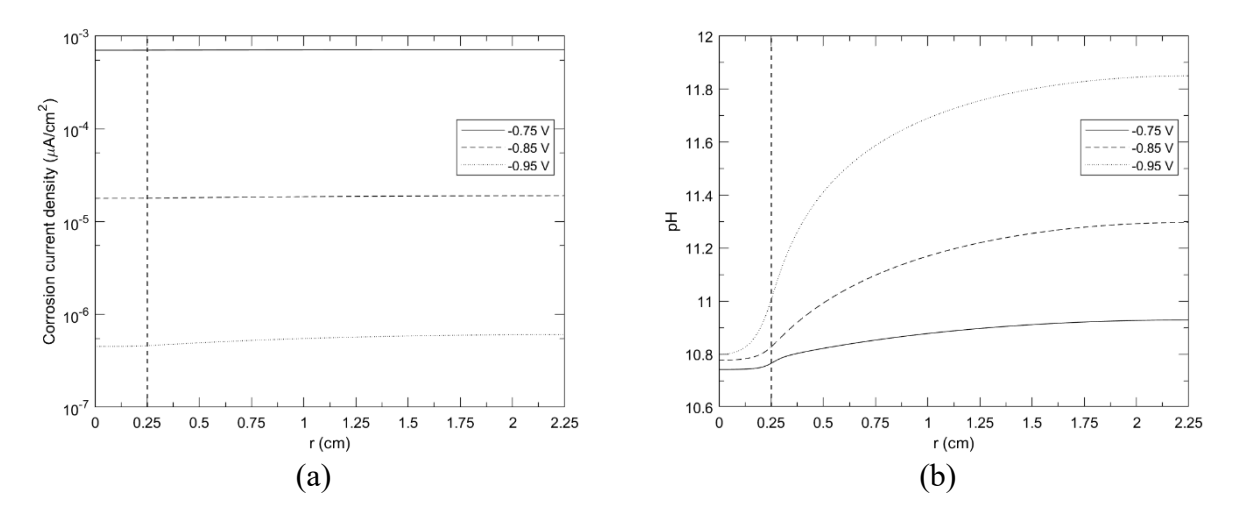


**Figure 14.** Influence of CP potential on corrosion current density and pH distribution as a function of position on the metal surface (a) corrosion current density distribution (b) pH distribution.

# (2) Disbondment length

The disbondment length represents the extent of coating failure and strongly influences corrosion and local chemistry. **Figure 15** shows the effect of disbondment lengths of 1 cm, 2 cm, and 3 cm on corrosion current density and pH distribution. Increasing disbondment length causes the corrosion current density in the disbonded region to rise more steeply with distance from the holiday, while the holiday area itself remains nearly unchanged. Similarly, longer disbondment leads to higher pH and a sharper alkaline gradient inside the disbonded zone. These results indicate that as the disbondment grows, protective current becomes less effective deeper inside, and the increasingly alkaline environment may accelerate further coating detachment.

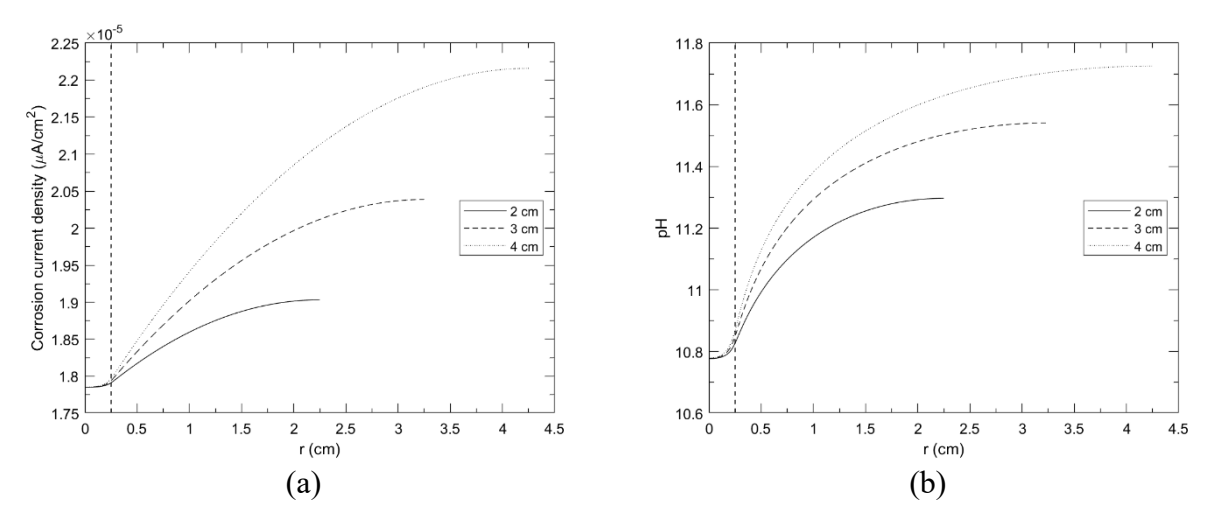


**Figure 15.** Influence of disbondment length on corrosion current density and pH distribution as a function of position on the metal surface (a) corrosion current density distribution (b) pH distribution.

# (3) Disbondment gap

The disbondment gap is the main pathway for cathodic protection current and species exchange between the holiday and the disbonded region. **Figure 16** shows the effect of gaps of 0.03 cm, 0.05 cm, and 0.07 cm on corrosion current density and pH distribution. Narrower gaps lead to a steeper increase in corrosion current density within the disbonded area, indicating reduced CP effectiveness due to limited current access. Local pH also rises with decreasing gap size, as restricted space slows hydroxide diffusion and causes stronger alkalinity. In contrast, the holiday region is little affected by gap size, with current density and pH remaining nearly unchanged.

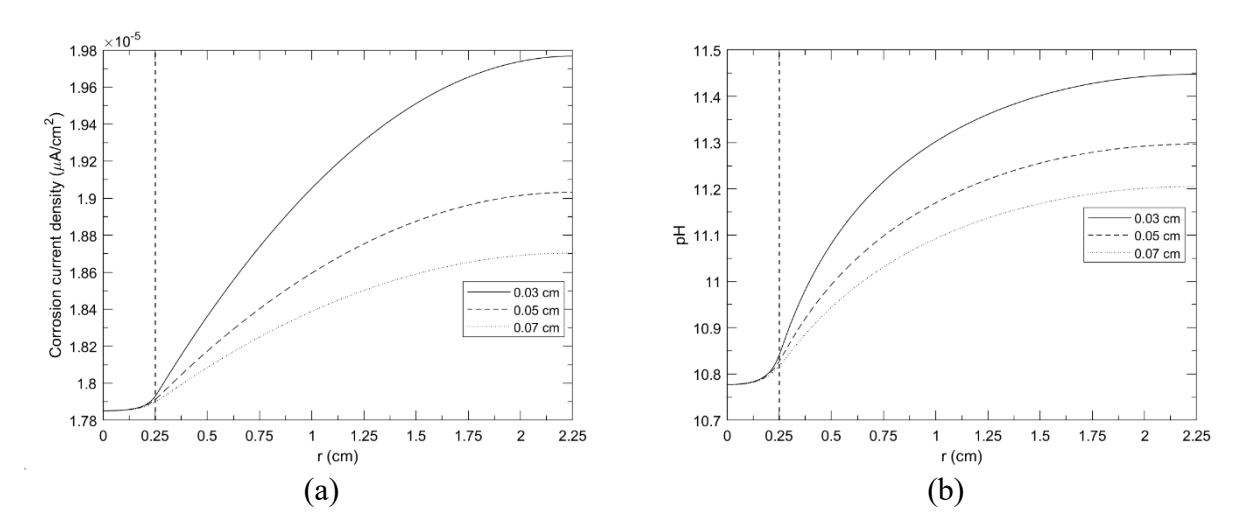


**Figure 16.** Influence of disbondment gap on corrosion current density and pH distribution as a function of position on the metal surface (a) corrosion current density distribution (b) pH distribution.

# (4) Soil resistivity

Soil resistivity critically governs the distribution and effectiveness of CP current. Figure 17 presents the influence of three representative resistivity levels on corrosion current density and pH distribution. Increasing resistivity results in a steeper radial increase of corrosion current density within the disbonded region, indicating diminished CP current penetration and reduced protective efficiency. Conversely, lower resistivity facilitates more uniform current distribution, reflected by flatter current density profiles. A similar trend is observed for pH: lower resistivity leads to a more alkaline environment throughout the interface due to enhanced cathodic reactions and greater hydroxide ion generation. These findings demonstrate that elevated soil resistivity can significantly impair CP performance and promote electrochemical conditions conducive to coating disbondment.

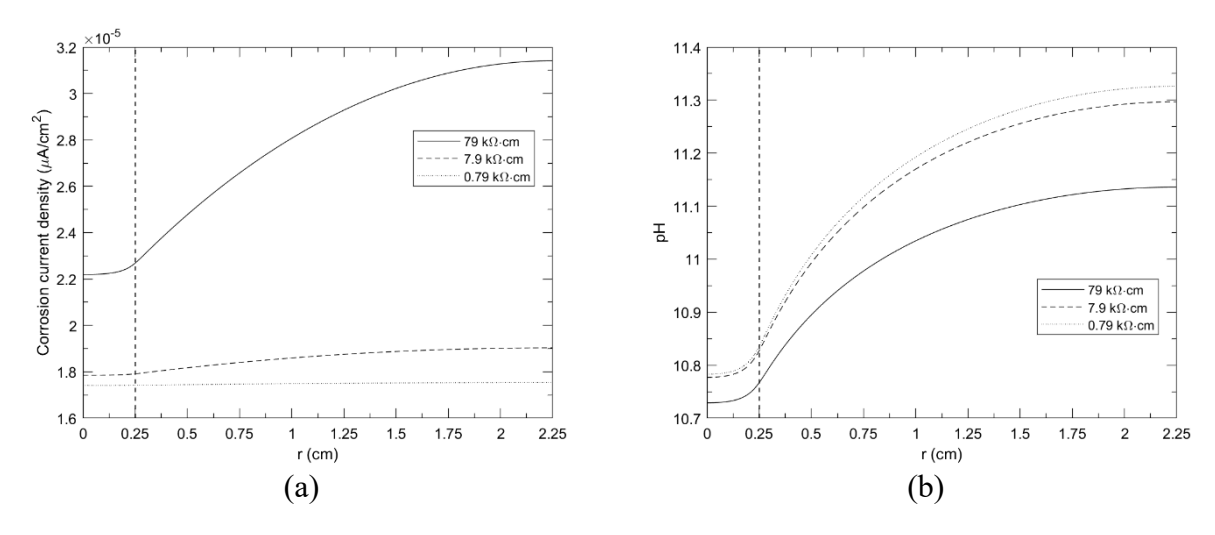


**Figure 17.** Influence of soil resistivity on corrosion current density and pH distribution as a function of position on the metal surface (a) corrosion current density distribution (b) pH distribution

# (5) Oxygen concentration

Dissolved oxygen availability directly controls the rate of the oxygen reduction reaction (ORR), a key cathodic process influencing CP performance. Figure 18 shows the effect of three oxygen concentrations on corrosion current density and pH distribution. Elevated oxygen levels intensify corrosion current density within the disbonded region, indicating stronger ORR activity and reduced CP effectiveness. Higher oxygen also leads to greater hydroxide generation, producing a more alkaline environment that can promote disbondment progression. Additionally, the pH distribution becomes more uniform under high oxygen conditions because vigorous ORR near the holiday increases initial hydroxide production, and subsequent migration and diffusion spread alkalinity deeper into the crevice.

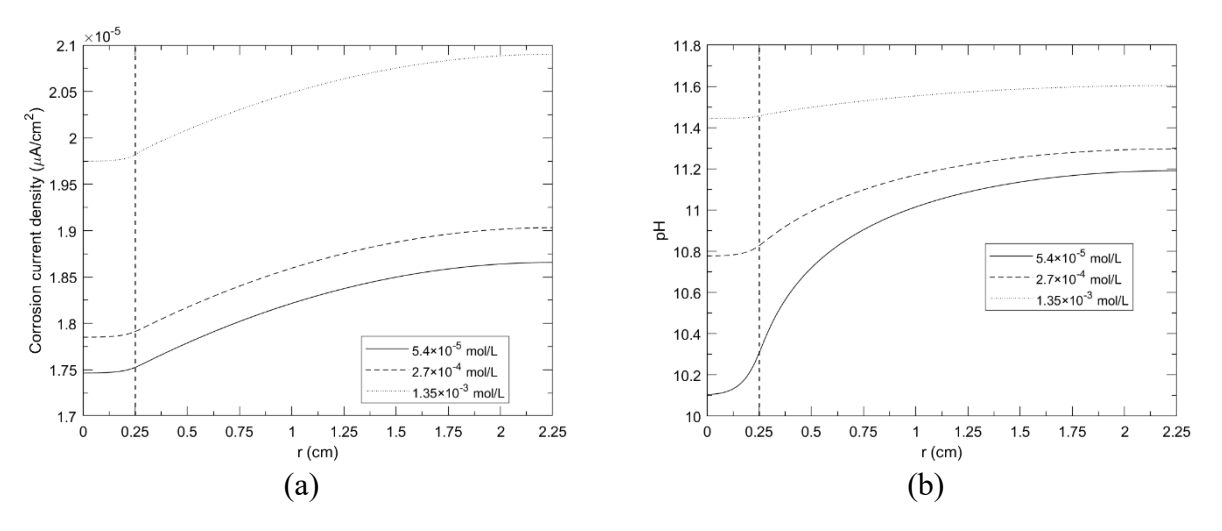


**Figure 18.** Influence of bulk oxygen concentration on corrosion current density and pH distribution as a function of position on the metal surface (a) corrosion current density distribution (b) pH distribution.

#### 3.3. Conclusions and Future Work

With the developed model, the main outputs include CP potential distribution, local current density for assessing local corrosion, and pH distribution for assessing coating disbandment potential. In the model design, the following parameters will be altered to study the effects of these variations on the outputs.

In this phase of the work, the model was developed and validated against experimental DC current measurements, showing good agreement across various coatings and CP levels. This verification confirms the model's predictive capability for assessing local corrosion and coating disbondment under different protective and environmental scenarios.

Building on this, the sensitivity analysis identified applied CP potential, disbondment length and gap, soil resistivity, and oxygen concentration as the most influential factors governing CP current distribution and local alkalinity. Understanding the relative impact of these parameters provides practical guidance for optimizing CP design and predicting disbondment progression.

Future work will focus on extending the current model to quantify local electrochemical conditions under various disbondment scenarios, particularly focusing on pH evolution and localized residual corrosion that can persist after coating failure. Those values are difficult to measure experimentally due to the small dimensions of the disbonded regions.

# 4. Task 4. Probabilistic Degradation Model of Coated Pipe Wall Due to Excessive CP

# 4.1. Background and Objectives in the 3<sup>rd</sup> Annual Report Period

Cathodic protection (CP) may lead to the degradation of coated steel pipelines; this degradation process can be considered as a stepwise mechanism, where the total degradation of the coated steel is the combination of the gradual evolution of different degradation processes. The first of these processes is the adhesion degradation of the steel coating, which is known as cathodic disbondment (CD). Once the disbondment is present, a degradation corrosion process in steel under disbonded coatings (CUDC) also takes part, simultaneously. Finally, once the coating is completely degraded, a direct corrosion process on the steel is expected.

The previous report described the philosophy behind the 3 degradation models to be considered in the prediction of the full degradation process of coated steel pipes. The objective of Task 4 in this reporting period is to report preliminary results for Model 1: coating disbondment (CD) based on information extracted from collected experimental data.

The degradation process of coated steel pipes can be considered the result of a gradual evolution of different processes, in consequence, this study assesses the total degradation (coating disbondment along with steel corrosion) by the assembly of three individual models: model for coating disbandment (Model 1), model for steel corrosion under CP (Model 2), and model for CP level on steel considering coating disbondment (Model 3).

# 4.2. Research Progress in the 3<sup>rd</sup> Annual Report Period

# 4.2.1. Model 1: prediction on coating disbondment rate

This degradation model will focus on predicting the level of coating disbondment degradation. Based on the data reported in the previous report and the extra data collected in this period, the level of degradation will be defined by the coating degraded area as a function of the CP level applied (noted as  $CP_{applied}$ ) by the cathodic protection. Previous experimental studies have used different CD standardized tests to evaluate resistance to CD of different coating types [4-7]. Literature review is used to collect coating disbondment data from different sources in order to assemble a database that covers a varied range of experimental conditions and coating types. A total of 260 data points representing three different coating types are obtained from 14 different experimental sources.

Disbondment radius/area has been used as the measurement of CD level. To compare CD results at different times between different studies, the cathodic disbondment rate (CD rate) is obtained by normalizing the disbondment results with respect to testing time. Then, for model development, the CD rate will be used as the response quantity to evaluate disbondment evolution over time.  $CP_{applied}$  potential, which refers to the CP level applied by the cathodic protection, is considered the main variable that influences the level of coating degradation. Coating thickness, coating type, carbon content on the steel coupon, electrolyte pH, temperature, and NaCl content are identified as additional variables reported and evaluated under different scenarios during CD testing. Table 4 summarizes these variables and their role during CD testing.

Table 4. Description of potential influencing variables obtained from experimental research.

Denomination	Variables	Description
$x_1$	Cathodic protection level, <i>CPapplied</i>	The level of cathodic protection applied to the coated pipeline is determined by the cathodic protection potential measurement. In pipelines, a high CP level may result in the formation of subproducts that can affect the adhesion of the coating around the defect and cause CD in coated pipelines. Disbondment areas increase as the applied absolute CP potential value increases [4, 6, 8].
$x_2$	Coating type	As a parameter linked to the coating's inherent characteristics, coating type is expected to significantly influence its resistance to CD. Coatings with different chemical compositions may have different disbondment responses to the same CP potential and testing conditions.
$x_3$	Coating thickness, t	Parameter related to the coating type. Previous studies have performed CD testing on coatings with different thicknesses [5-7], based on the belief that CD rate decreases with thicker film coating, based on the assumption that CP coating permeability is affected by the increase of coating thickness [9].
<i>X</i> 4	Electrolyte pH, <i>pH</i>	This parameter refers to the pH level in the electrolyte around the holiday during CD testing [4, 5, 10]. It has been previously reported that the cathodic reaction can produce subproducts with high pH (alkaline), and these subproducts, located under the coating, can lead to disbonding [8].
<i>x</i> <sub>5</sub>	Temperature, T	Some experimental studies on CD have reported an increase in the surface area of disbonded coating on tests performed at temperatures higher than room temperature. Increasing temperature may lead to accelerating cathodic reactions and to an increase in electric current, leading to an acceleration of the disbanding rate.
<i>x</i> <sub>6</sub>	Carbon content on steel coupon, C	As mentioned before, cathodic overprotection can result in the formation of subproducts that affect the coating adhesion. The influence of these subproducts may vary based on the steel coupon composition, which includes the steel carbon content.
<i>x</i> <sub>7</sub>	NaCl content in the electrolyte, NaCl	CD standard test methods are carried out on samples immersed in a 3% sodium chloride ( <i>NaCl</i> ) electrolyte (solution); however, some modified tests have experimented with different <i>NaCl</i> concentrations in order to identify possible changes in the chemical process that can lead to changes in the CD rate.

All the variables reported in Table 4 were originally considered as independent variables in Model 1 development, which aims to predict the change in CD rate,  $r_{CD}$ . A multilinear regression is adopted to formulate this model, as shown below:

$$\log(r_{CD}) = \beta_0 + \sum_i \beta_i \cdot x_i + \varepsilon \tag{12}$$

where  $x_i$  (i = 1,...,n) = model predictors,  $\beta_i$  (i = 0,...,n) = regression coefficients, and  $\epsilon \sim N(0, \sigma^2)$  = model error. The experimental CD rates from the collected database are used to estimate the unknown parameters (i.e.,  $\beta_i$  and  $\sigma$ ). Logarithm transformation of  $r_{CD}$  is used in **Equation 12** to satisfy the assumptions implied in the regression: model error ( $\epsilon$ ) distribution has mean zero and variance of  $\epsilon$  is constant; and using logarithm transformation of  $r_{CD}$  also ensures the predicted  $r_{CD}$  will always be positive. A model selection process is carried out to identify the predictors that have a significant contribution to the model prediction. The variable selection adopted here is a stepwise forward regression based on the probability value results (p-values) of each variable.  $R_{adj}^2$  is used to measure the fitting quality of the model.

The database contains missing data, which represents instances where a variable's value was not reported in the experimental study. Consequently, if a variable with missing values is included during model selection, the corresponding data points will be removed from the training set, leading to a reduction in the overall database size. Considering this, four variables were selected for the model prediction, with a database size equal to 141 datapoints. Consequently, the prediction model for  $r_{CD}$  with the best performance after model selection is given by:

$$\log(r_{CD}) = \beta_0 + \beta_1 \cdot x_1 + \beta_2 \cdot x_2 + \beta_3 \cdot x_3 + \beta_4 \cdot x_2 \cdot x_3 + \beta_5 \cdot x_3 \cdot x_5 + \varepsilon \tag{13}$$

**Figure 19** shows the predicted CD rate vs. actual CD rate in logarithm space, where the solid line shows the unit line and dotted line shows  $\pm 1\,\sigma$ , and the points denoted as starts are the testing data (that are the experimental data from CD testing in Task 2 conducted by The University of Akron, consisting of 65 data points for two coating types, FBE and Liquid Epoxy coatings). **Figure 19** shows that the performance of the predictive model on training data (denoted by non-star symbols) is decent, with most of those data points within the dotted lines and evenly distributed over the solid line. However, the model does not yield unbiased predictions for testing data, indicated by the uneven distribution of data points relative to the unit line. Additionally, a clear clustering pattern is evident based on the coating type, with distinctly better predictive accuracy observed for FBE coatings than for Liquid and Solid epoxy.

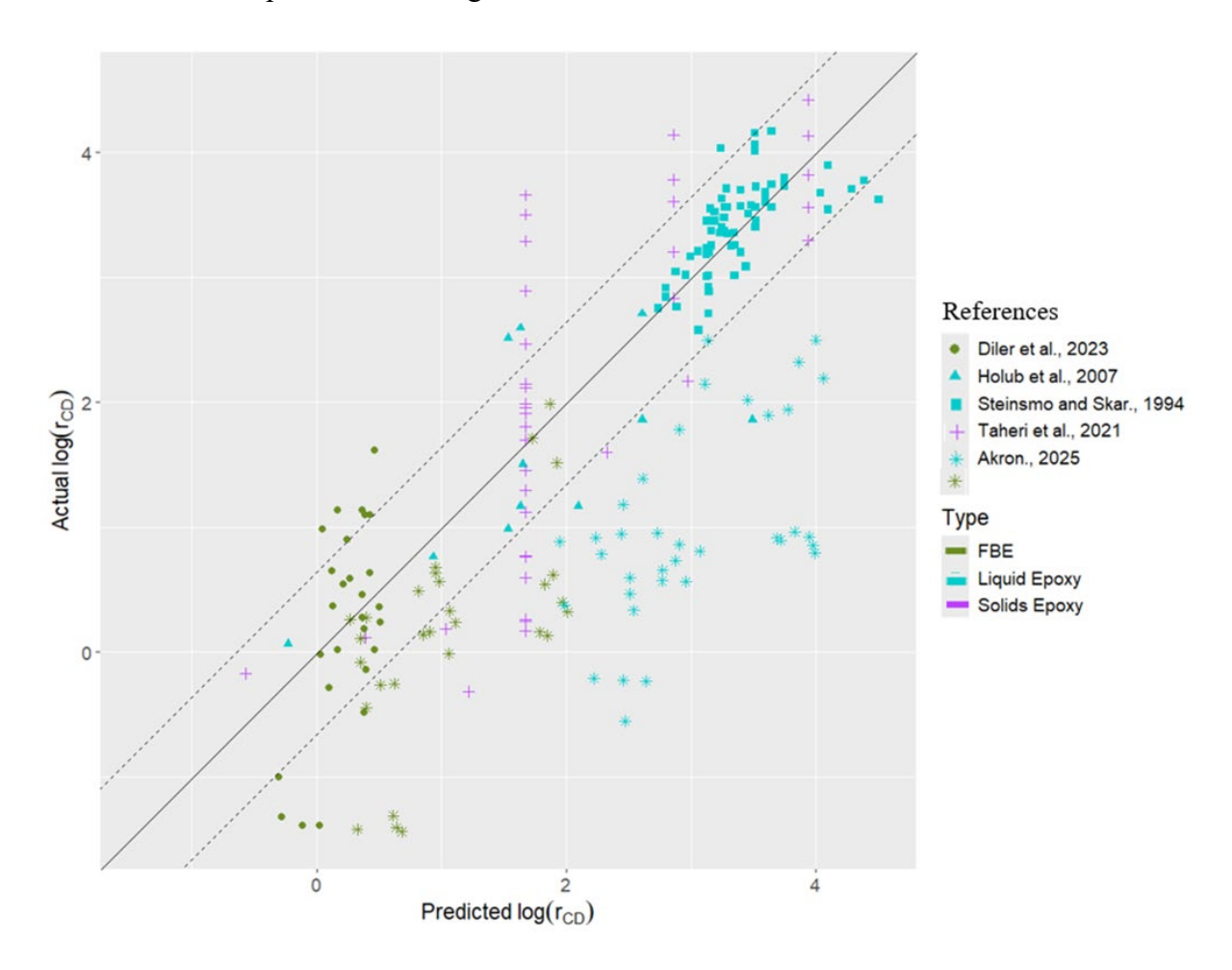
A closer analysis was conducted to examine the influence of predictor variables on the CD rate across three different coating types. **Figure 20** shows the relationships between the three variables  $(CP_{applied}, \text{ coating thickness}, \text{ and temperature})$  used in the model and the CD rate based on the data reported from experimental studies. Those relationships show different trends for the three coating types. These different correlations suggest that the influence of the predictor variables on the CD rate is dependent on the coating type and its properties.

These results lead us to consider cluster-wise regression as the next step in the prediction model development. Cluster-wise regression is a statistical modeling technique that analyzes data with underlying clustering patterns by classifying the data and performing regression/prediction on small subsets, thereby accounting for the internal correlation within clusters. Two of the machine learning models available for cluster-wise regression are:

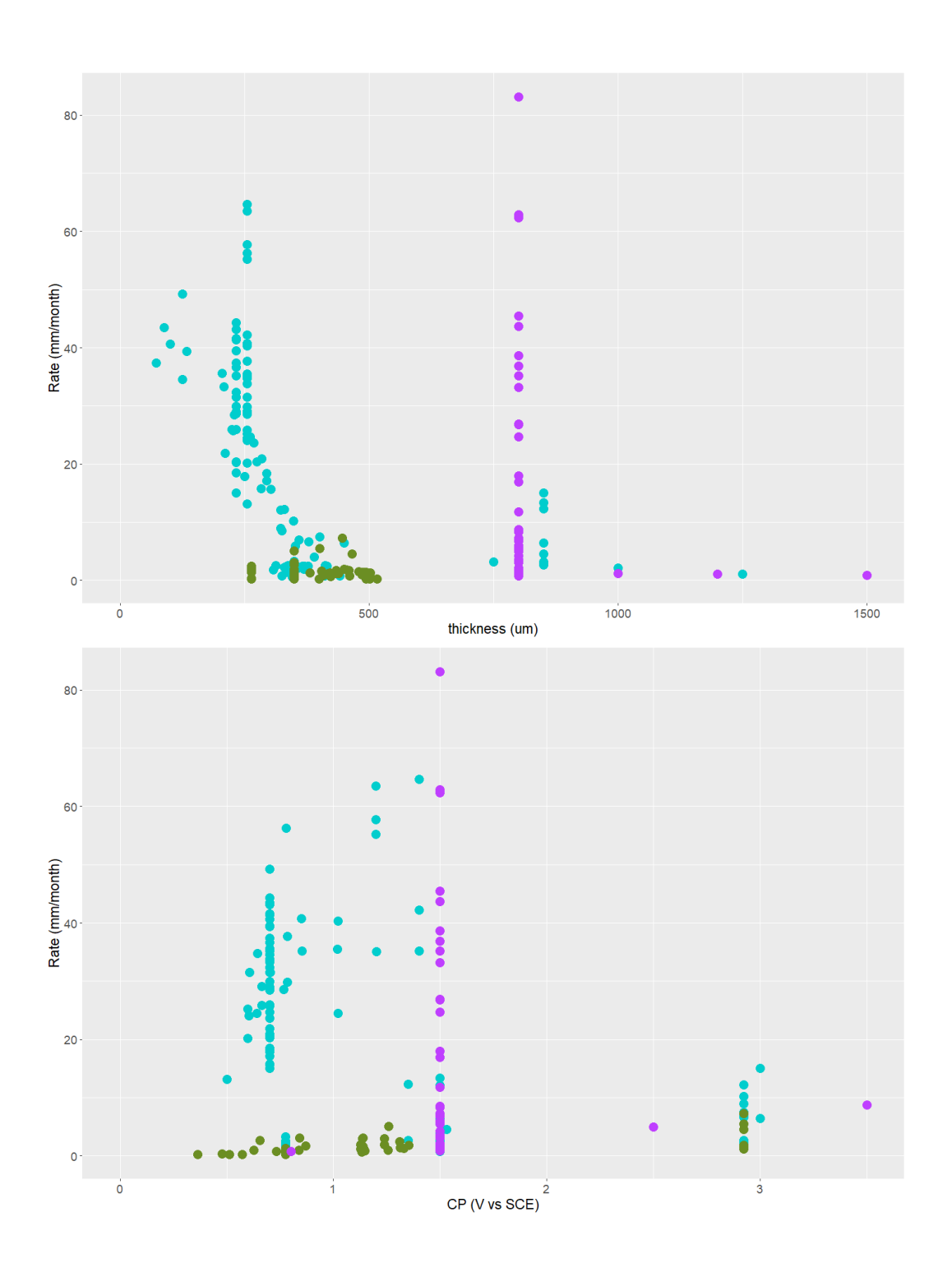
• Clustered linear regression: Clustered linear regression (CLR) is a new machine learning

algorithm that improves the accuracy of classical linear regression by partitioning the training space into subspaces [11]. The model goal is to first perform classification by partitioning the data into a given number of clusters and to find regression coefficients for each cluster.

• Regression Tree: Regression tree models deliver predictions based on partitioning the data into smaller, more homogeneous groups, subsets on specific feature thresholds [12]. Once the tree is built, a new data point is passed down the tree, following the split rules until it reaches a node. The predicted outcome for that data point is the constant average value of the target variable in that specific node. Regression trees do not offer a close-formed model.



**Figure 19.** Unit plot of the CD rate predictions by the proposed model (Predicted) vs the experimental data (Actual).



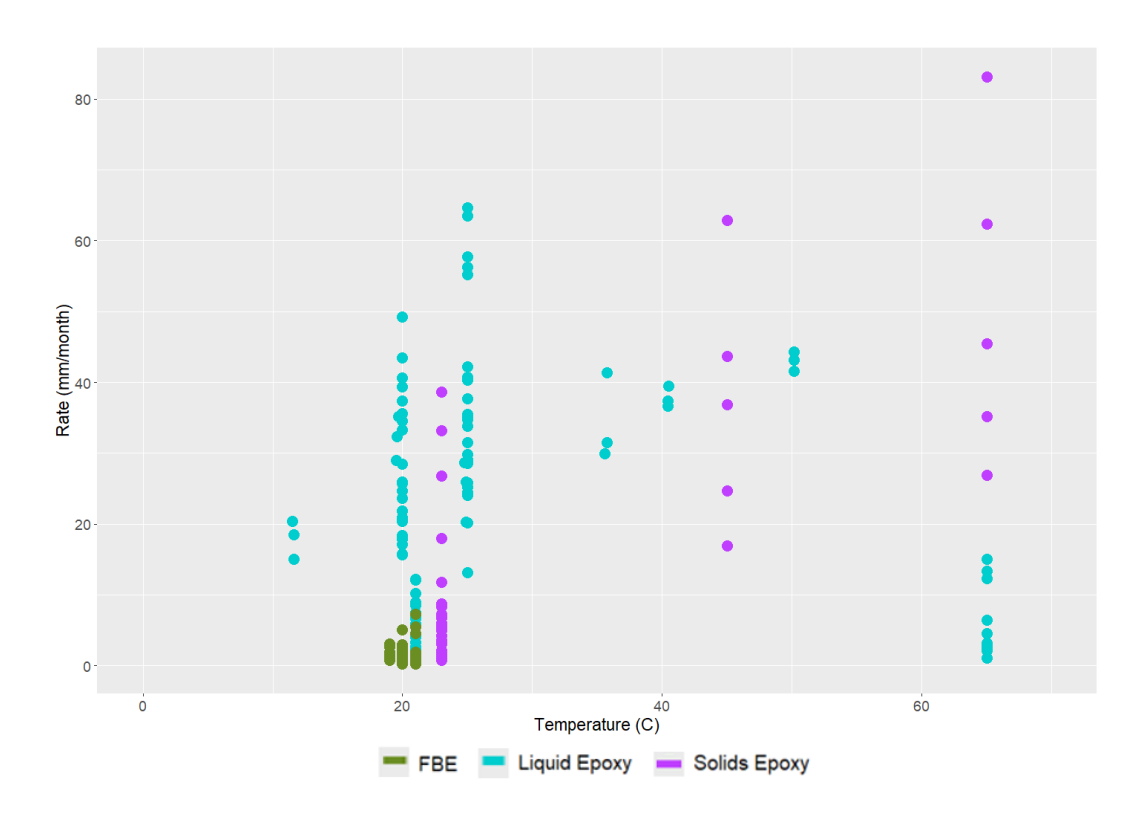


**Figure 20.** Correlation between regression variables considered in multilinear regression and CD rate

# 4.2.2. Model 2: prediction on steel corrosion rate

From the cathodic protection technique, it is widely accepted that the CP level is directly related to the protection level against corrosion reached by the steel pipe; a decrease in the level of protection can represent a direct effect on the corrosion rate. Through the shielding effect, the CD degradation process can affect the amount of current passing through the disbonded coating, directly affecting the effective level of CP that reaches the steel surface [4, 5, 8]. The CP level applied ( $CP_{applied}$ ) as a protective system can be partially permeable. If the CP level potential is low (e.g., -0.85 V(CSE)), the CP current cannot provide full protection to the steel in corrosive environments trapped under the disbonded coating [5]. The second degradation model will aim to establish the level of steel pipe corrosion degradation, once the CD effect is present, as a function of the effective CP level applied to the steel, noted as  $CP_{steel}$ . Clearly, when coating is completely degraded or coating is absent,  $CP_{applied} = CP_{steel}$ .

To develop this model, data that contains corrosion rate and  $CP_{steel}$  will be needed. As an example, **Figure 21** shows the correlation between corrosion rate and  $CP_{steel}$  using the data collected [9, 10, 13] during this report period. More data from experimental studies is currently being collected for model development. Other potential variables on the corrosion rate are metal types, steel decomposition, and environmental factors.

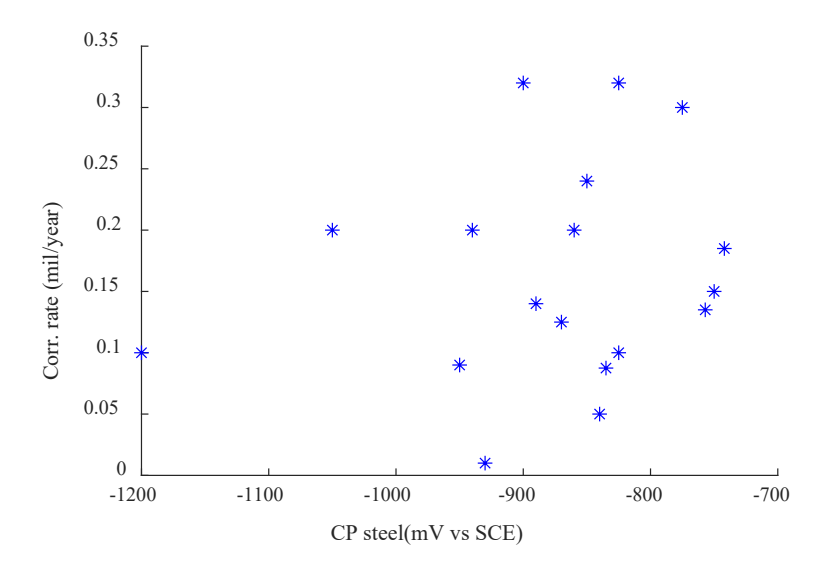


**Figure 21.** Correlation between corrosion rate and  $CP_{steel}$ .

## 4.2.3. Model 3: prediction on the CP level on steel under coating disbondment

In the presence of cathodic disbondment, the effective level of cathodic protection on steel ( $CP_{steel}$ ) can be significantly different from the CP level initially applied,  $CP_{applied}$ , from the cathodic protection system. This change can be explained by the cathodic shielding effect; however, previous experimental studies have evaluated the change in the effective CP level under disbonded coatings and identified additional factors with a correlation to the effective CP level reached at the steel surface [4-8, 13]. Using simulated coating disbondment on steel coupons, CP currents were applied to the open mouth of the simulated coating disbondment, and the CP effective level at different locations in the coating disbondment was monitored. Data collected from experimental studies have shown that holiday geometry, including distance from the open mouth (OM) and the disbondment gap size, as well as the steel type (steel grade), present correlations with the changes in the effective CP.

From the data collected so far, a change in the effective level of CP (negative  $\Delta CP = CP_{applied} - CP_{steel}$ ) was observed at different locations from the open mouth and different disbondment gap sizes. Figure 22(a) is a 3D sample representation that shows the variation in  $\Delta CP$  at different distances from the OM and different gap sizes for different steel grades. Figure 22(b) shows the direct correlation between  $\Delta CP$  and distance from the OM. In general, a decrease in  $\Delta CP$  is observed for all coatings exposed as the distance from the OM increases, regardless of the crevice gap value. In Figure 22(c), similar behavior is observed for  $\Delta CP$  regardless of the coating type. Finally, Figure 22(d) shows the direct correlation between  $\Delta CP$  and crevice gap values. The plot shows a decreasing tendency for  $\Delta CP$  as the crevice gap increases due to the shielding effect. The variations in those plots may be due to the influence of other factors, such as steel decomposition and environmental factors. For example, different values of  $\Delta CP$  are observed for the same crevice gap value and the same steel, particularly for X65, as shown in Figure 22(d). Thus, all possible influencing factors should be holistically considered in model development.

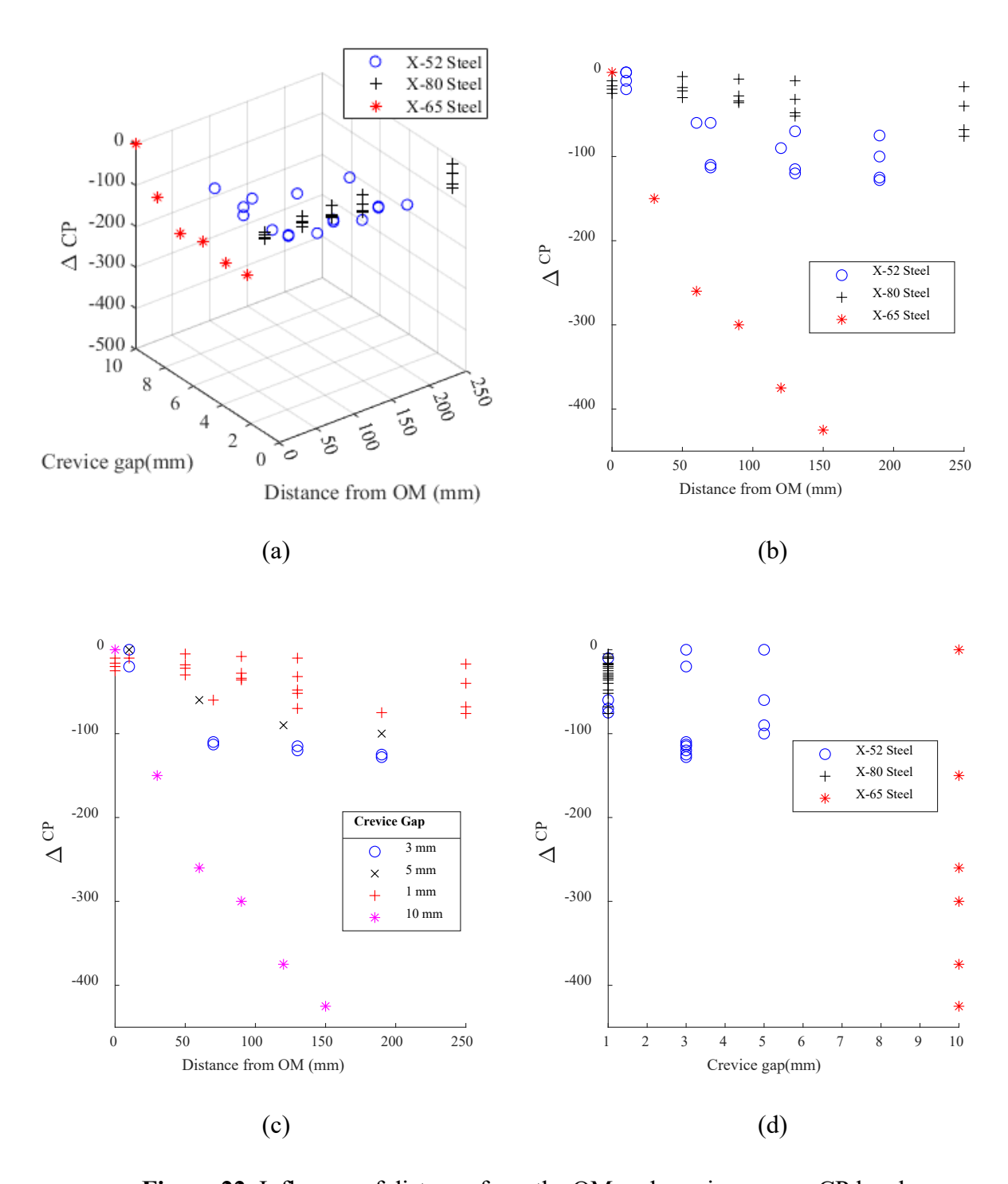


Figure 22. Influence of distance from the OM and crevice gap on CP level.

#### 4.3. Conclusions

Based on these preliminary results for Model 1, multilinear regression models proved to be not accurate enough to predict CD rate on pipelines due to the different relationships between variables and CD rate for each coating type. These results lead us to consider cluster-wise regression as the

next step in the prediction model development. Cluster-wise regression is a statistical modeling technique that analyzes data with underlying clustering patterns by classifying the data and performing regression/prediction on small subsets, thereby accounting for the internal correlation within clusters.

#### 4.4. Future Work

The following activities will be conducted in the future:

- Cluster-wise model development of Model 1: clustered linear regression and regression tree models will be developed and compared.
- Model development of Model 2 using multivariable linear regression
- To expand data collection for Model 3 and conduct model development

# 5. Task 5. Determination of Recoating Time Using Reliability-based Approach

Task 5 will start when Task 4 is completed.

#### 6. Task 6. Industrial Collaborations

The PIs contacted external partners from the oil and gas pipeline industry for industrial collaborations during this reporting period. We sent a survey to pipeline companies to acquire field information. We also talked to experts in pipelines at the annual 2025 AMPP conference. We provided our up-to-date research outcomes to the PRCI Corrosion Technical Committee for their comments and feedback.

We received vintage pipes with coating from Dr. Rafael Rodriguez through his company. Dr. Rodriguez kindly provided us with the CP operation potential and coating information for these pipe samples.

# References

- [1] N. Leslie, J. Mauzeroll, Spatially resolved electrochemical measurements, in: K. Wandelt, G. Bussetti (Eds.) Encycl. Solid-Liq. Interfaces, Elsevier, Oxford, 2024, pp. 461–478.
- [2] R. Ghamsarizade, B. Ramezanzadeh, H.E. Mohammadloo, Chapter 12 Corrosion measurements in coatings and paintings, in: J. Aslam, C. Verma, C.M. Hussain (Eds.) Electrochem. Anal. Tech. Sustain. Corros. Monit., Elsevier, Oxford, 2023, pp. 217–264.
- [3] J. Zhang, Z. Li, W. Sun, X. Li, M. Cui, E. Zhou, F. Wang, D. Xu, Extracellular polysaccharides of Tenacibaculum mesophilum D-6 play a major role during its corrosion protection for X80 carbon steel in seawater, Corrosion Science, 249 (2025) 112811.
- [4] F. Varela, M.Y.J. Tan, M. Forsyth, Understanding the effectiveness of cathodic protection under disbonded coatings, Electrochimica Acta, 186 (2015) 377-390.
- [5] O.Ø. Knudsen, U. Steinsmo, Effects of cathodic disbonding and blistering on current demand for cathodic protection of coated steel, Corrosion, 56 (2000) 256-264.
- [6] M. Latino, F. Varela, M.Y.J. Tan, M. Forsyth, An overview on cathodic shielding produced by disbonded coatings, Corrosion & Prevention, (2016).
- [7] N. Guermazi, A. Ibrahmi, H. Hmidi, K. Elleuch, H.F. Ayedi, Susceptibility to corrosion damage of pipeline steels under coating disbondments, Materials and Corrosion, 61 (2010) 43-50.
- [8] M.Y. Tan, F. Bob Varela, Y. Huo, An overview of recent progress in probing and understanding corrosion under disbonded coatings, Corrosion Engineering, Science and Technology, 58 (2023) 323-332.
- [9] F.M. Song, N.J.C.S. Sridhar, Modeling pipeline crevice corrosion under a disbonded coating with or without cathodic protection under transient and steady state conditions, Corrosion Science, 50 (2008) 70-83.
- [10] H. Najafi, A. Eslami, M.A. Golozar, A. Kavian, M. Ahmadi, Effect of pulse cathodic protection on corrosion mitigation and electrochemical conditions under a simulated coating disbondment on pipeline steel, Materials and Corrosion, 73 (2022) 116-124.
- [11] B. Ari, H.A. Güvenir, Clustered linear regression, Knowledge-Based Systems, 15 (2002) 169-175.
- [12] K. Joki, A.M. Bagirov, N. Karmitsa, M.M. Mäkelä, S. Taheri, Clusterwise support vector linear regression, European Journal of Operational Research, 287 (2020) 19-35.
- [13] R. Ashari, A. Eslami, M. Shamanian, Corrosion and electrochemical conditions of pipeline steel under tape coating disbondments: effect of disbondment gap size and morphology, Journal of Pipeline Systems Engineering and Practice, 11 (2020) 04019051.